PROPAGATION OF A CHEMICAL REACTION THROUGH HETEROGENEOUS LITHIUM-POLYTETRAFLUOROETHYLENE MIXTURES

Richard B. Smith

Pennsylvania State University

Prepared for:

Naval Sea Systems Command

11 December 1975

PROPAGATION OF A CHEMICAL REACTION THROUGH HETEROGENEOUS LITHIUM-POLYTETRAFLUOROETHYLENE MIXTURES

Richard B. Smith

Technical Memorandum
File No. TM 75-302
December 11, 1975
Contract No. N00017-73-C-1418

Copy No. 62

The Pennsylvania State University
Institute for Science and Engineering
APPLIED RESEARCH LABORATORY
Post Office Box 30
State College, PA 16801

NAVY DEPARTMENT

NAVAL SEA SYSTEMS COMMAND

UNCLASSIFIED
SECURITY CLASSIFICATION OF THIS PAGE (When Data Entered)

REPORT DOCUMENTATION PAGE		READ INSTRUCTIONS BEFORE COMPLETING FORM
1. REPORT NUMBER TM 75-302	2. GOVT ACCESSION NO.	3. RECIPIENT'S CATALOG NUMBER
4. TITLE (and Subtitle) PROPAGATION OF A CHEMICAL REACTION THROUGH HETEROGENEOUS LITHIUM-POLYTETRAFLUOROETHYLENE MIXTURES		5. TYPE OF REPORT & PERIOD COVERED Ph.D. Thesis, March 1976 6. PERFORMING ORG. REPORT NUMBER TM 75-302
7. AUTHOR(s) Richard B. Smith		8. CONTRACT OR GRANT NUMBER(s) N00017-73-C-1418
9. PERFORMING ORGANIZATION NAME AND ADDRESS The Pennsylvania State University Applied Research Laboratory P. O. Box 30, State College, PA 16801		10. PROGRAM ELEMENT, PROJECT, TASK AREA & WORK UNIT NUMBERS
11. CONTROLLING OFFICE NAME AND ADDRESS Naval Sea Systems Command Department of the Navy Washington, D. C. 20362		12. REPORT DATE December 11, 1975 13. NUMBER OF PAGES ~~126 pages and figures~~ 128
14. MONITORING AGENCY NAME & ADDRESS(if different from Controlling Office)		15. SECURITY CLASS. (of this report) Unclassified, Unlimited 15a. DECLASSIFICATION/DOWNGRADING SCHEDULE

16. DISTRIBUTION STATEMENT (of this Report)

Approved for public release, distribution unlimited,
per NSSC (Naval Sea Systems Command), 1/29/76

17. DISTRIBUTION STATEMENT (of the abstract entered in Block 20, if different from Report)

18. SUPPLEMENTARY NOTES

19. KEY WORDS (Continue on reverse side if necessary and identify by block number)

CHEMICAL REACTION
HETEROGENEOUS MIXTURES
LITHIUM POLYTETRAFLUOROETHYLENE
PROPAGATION VELOCITY
REACTION PREDICTION
REACTION RATE
THERMAL DECOMPOSITION

20. ABSTRACT (Continue on reverse side if necessary and identify by block number)

An analytical and experimental investigation of the propagation of a chemical reaction through heterogeneous lithium-polytetrafluoroethylene (PTFE) mixtures was conducted. PTFE in the form of both solid rod and resin was reacted with lithium, these reactants being initially at room temperature and under a vacuum. The reaction sample was of cylindrical geometry with the PTFE located along the longitudinal centerline. The chemical reaction was initiated at one end of the sample, and the motion

DD FORM 1 JAN 73 1473 EDITION OF 1 NOV 65 IS OBSOLETE

UNCLASSIFIED
SECURITY CLASSIFICATION OF THIS PAGE (When Data Entered)

of the propagating reaction front was monitored by means of thermocouples located at the lithium-PTFE interface. A two-dimensional model was developed based on the assumptions that the reaction rate controlling process was the thermal decomposition of the PTFE, that the reaction products were in the condensed phase, and that conduction was the sole mode of heat transfer. The dimensionless form of the model was solved numerically, and the predicted reaction propagation velocities were in reasonable agreement with experimental results.

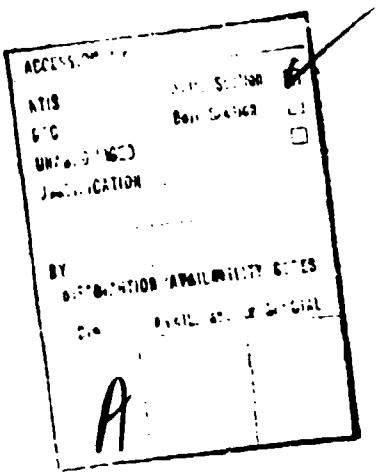

ACKNOWLEDGMENTS

The author wishes to express his sincere appreciation to his advisor, Professor Donald R. Olson, for his valuable advice, timely guidance, and continued encouragement throughout the course of this investigation.

He also desires to thank Dr. Laurence A. Ferris, of E. I. duPont de Nemours and Company, for his kind assistance in obtaining a portion of the PTFE used in the experimental program.

The author wishes to acknowledge the support for this investigation by the Applied Research Laboratory of The Pennsylvania State University under contract with the Naval Ordnance Systems Command.

TABLE OF CONTENTS

TABLE OF CONTENTS (CONTINUED)

LIST OF TABLES

LIST OF FIGURES

NOMENCLATURE

Symbol	Description
A^*	Dimensionless parameter defined by Equation (2.15)
A_o	Frequency factor in PTFE thermal decomposition rate law, Equation (2.4) (s^{-1})
C_1-C_{12}	Dimensionless constants defined by Equations (A.7), (A.17), (A.25) and (A.29)
C_p	Specific heat at constant pressure (J/kg - K)
E^*	Dimensionless parameter defined by Equation (2.15)
E_a	Activation energy in PTFE thermal decomposition rate law, Equation (2.4) (J/mol)
e	Natural logarithm base
F^*	Dimensionless parameter defined by Equation (2.15)
H^*	Dimensionless thickness of lithium-PTFE reaction sample
H_T^*	Dimensionless thickness of PTFE
ΔH_R	Standard heat of reaction (J/kg reactants)
h	Thickness (m)
K	Constant defined by Equation (4.1) (s)
k	Thermal conductivity (W/m-K)
L^*	Dimensionless length of lithium-PTFE reaction sample
ℓ	Length of lithium-PTFE reaction sample (m)
M^*	Dimensionless PTFE-lithium mass ratio
m	Mass of PTFE (kg)
m_o	Initial mass of PTFE (kg)
n_T	Number of Y* direction grid points in PTFE
n_T'	Number of Y* direction grid points in stoichiometric lithium
n_X	Number of X* direction grid points in lithium-PTFE reaction sample

NOMENCLATURE (CONTINUED)

Symbol	Description
$\dot{q}$	Rate of heat generation per unit volume (W/m^3)
R*	Dimensionless parameter defined by Equation (2.15)
R	Universal gas constant (J/mol - K)
T*	Dimensionless temperature defined by Equation (2.11)
T_o*	Dimensionless initial temperature
T	Temperature (K)
T_{af}	Adiabatic flame temperature of lithium-PTFE reaction at one atmosphere total pressure (K)
T_o	Initial temperature (K)
t	Time (s)
t_{ch}	Characteristic time required to thermally decompose 90% of an initial amount of PTFE at T_{af} (s)
V*	Dimensionless reaction propagation velocity defined by Equation (2.26)
V_{ch}	Characteristic velocity defined by Equation (2.27) (m/s)
W	Ratio of mass of reactants consumed to mass of PTFE thermally decomposed
X*	Dimensionless coordinate parallel with direction of reaction front propagation, defined by Equation (2.11)
ΔX*	Dimensionless X* direction grid spacing
XS	Number of moles of lithium present in reaction sample in excess of that required by stoichiometry
x	Coordinate parallel with direction of reaction front propagation (m)
Y*	Dimensionless coordinate perpendicular to direction of reaction front propagation, defined by Equation (2.11)
ΔY*	Dimensionless Y* direction grid spacing
y	Coordinate perpendicular to direction of reaction front propagation (m)

NOMENCLATURE (CONTINUED)

Symbol	Description
Z^*	Mass fraction
α	Thermal diffusivity (m^2/s)
ρ	Density (kg/m^3)
τ^*	Dimensionless time defined by Equation (2.11)

Subscripts

i	Pertains to a specific grid point
j	Pertains to a specific grid point
L	Pertains to lithium
LS	Pertains to stoichiometric lithium
LT	Pertains to lithium-PTFE interface
LX	Pertains to excess lithium
P	Pertains to reaction products
S	Pertains to steady conditions
T	Pertains to PTFE

Superscript

N	Pertains to dimensionless time level

CHAPTER I

INTRODUCTION

1.1 General Statement of the Problem

The past decade has witnessed a vast intensification in the search for new sources of energy in the form of heat. In many applications such as electric power generation, supply, cost, and environmental considerations are of primary concern in the selection of a heat source. Space, underwater, and several other applications, however, dictate that high energy density is of the utmost importance, energy density being defined as the amount of heat generated per unit weight of fuel and oxidizer consumed. The chemical reactions between the alkali metals and the halogen gases are all quite attractive from an energy density standpoint, and of these several possible fuel-oxidizer combinations, the reaction between lithium and fluorine produces the largest amount of heat per unit weight of reactants.

Lithium is the lightest known metal, and is relatively plentiful. Although it is extremely reactive at elevated temperatures, lithium may be handled with reasonable ease and safety at temperatures up to slightly above its melting point, 454 K. Fluorine, on the other hand, is exceedingly toxic and very difficult to handle under all conditions. The highly fluorinated polymers such as polytetrafluoroethylene, PTFE (Teflon*, Fluon**, Halon***), however,

---

*Registered trademark, E.I. duPont de Nemours and Company
**Registered trademark, ICI America Incorporated
***Registered trademark, Allied Chemical Corporation

provide a convenient, safe, and inexpensive source of fluorine. PTFE, chemical formula nC_2F_4, is 76% fluorine by weight, and in its solid form is slightly more dense in fluorine than is liquid fluorine at its normal boiling point. Available commercially in the form of rod, sheet, and resin, PTFE is known primarily for its chemical inertness. Product literature indicates that PTFE will react with the molten alkali metals, although information concerning the conditions under which the reaction might be initiated and the order of magnitude of the attendant rate is not available. Were it possible to initiate the lithium-PTFE reaction without undue effort, and were this reaction to proceed at a reasonably rapid rate, this reactant combination might well prove attractive in applications requiring a high energy density heat source. Therefore, some preliminary testing was undertaken in order that the answers to these questions might be ascertained.

At the outset of preliminary testing, it was decided that the configuration in which the lithium-PTFE reaction might be examined with the most generality was that of a flat circular wafer of lithium covered by the PTFE oxidizer. It was hoped that with the sample under an initial vacuum, the reaction could be ignited at the center of the wafer by means of an electrically heated wire, and allowed to propagate radially. Accordingly, some feasibility tests were run using a 25.4 mm diameter lithium wafer covered with PTFE resin. Although a considerable number of attempts at igniting the reaction with the electrically heated wire alone proved fruitless, it was found that by augmenting the hot wire with a small amount of monopropellant, the reaction could be ignited quite reliably. The volume of the

containment vessel used in these tests was only slightly greater than that required by the reactants; very little free volume was present above the sample.

The use of this experimental configuration having appeared feasible, a larger scale test apparatus to accommodate a 140 mm diameter lithium sample was constructed. In this device, a rather large free volume above the reaction sample was provided in order that test preparation might be facilitated. After the lithium wafer and the PTFE resin were installed, a thin stainless steel disc was placed on top of the PTFE resin. Thermocouples, which were intended to be used to monitor the position of the propagating reaction front, were inserted through holes placed in this disc at various radial and circumferential locations. The thermocouple measuring junctions were located at the lithium-PTFE interface. A larger hole was located at the center of the disc to provide an area for the ignition of the reaction. With this device, all attempts at initiating a self-propagating reaction under a vacuum with the monopropellant-augmented hot wire proved unproductive. In some cases the PTFE resin was seen to be blown away from the ignition area by the burning of the monopropellant; in others, the reaction appeared to have propagated a short distance and then stopped. In all cases, a considerable amount of material thought to be reaction products from the monopropellant was found in the free volume over the sample after ignition was attempted.

From the results of these tests, it was concluded that the lithium-PTFE reaction would not self-propagate in a radial manner, in which the surface area covered by the reaction front was forced to

increase during the propagation. For this reason, it was decided to continue preliminary testing in a cylindrical configuration, in which a constant reaction front surface area was maintained. Additionally, it was felt that the use of a commercially available igniter in place of the monopropellant-augmented hot wire would substantially improve the probability of a reliable ignition of the reaction.

An initial experiment involving lithium and PTFE resin in the cylindrical configuration was conducted in an apparatus as shown in Figure 1. The device consisted of a length of stainless steel tubing with a welded closure at one end and a tube fitting at the other. A commercially available lithium rod of 25.4 mm diameter and 203 mm length was inserted into this tube, and a 9.5 mm diameter hole along the longitudinal axis of the lithium rod was produced by driving a length of tubing through the lithium and removing the resulting slug. A quantity of PTFE resin was tamped into this hole, and an igniter was positioned at the upper end for the purpose of initiating the reaction. While these preparations were being carried out, an attempt was made to continuously bathe the sample in argon gas to minimize air contamination of the lithium. Thermocouples welded to the outside of the tube along its length were connected to a recording oscillograph in order that the motion of the reaction front might be monitored. Thermochemical calculations, based on the assumption of lithium fluoride and lithium carbide reaction products, indicated that sufficient excess lithium was present to limit the final mean temperature of the material within the tube, after the reaction had taken place, to a reasonable level of 1100-1150 K. Before the test

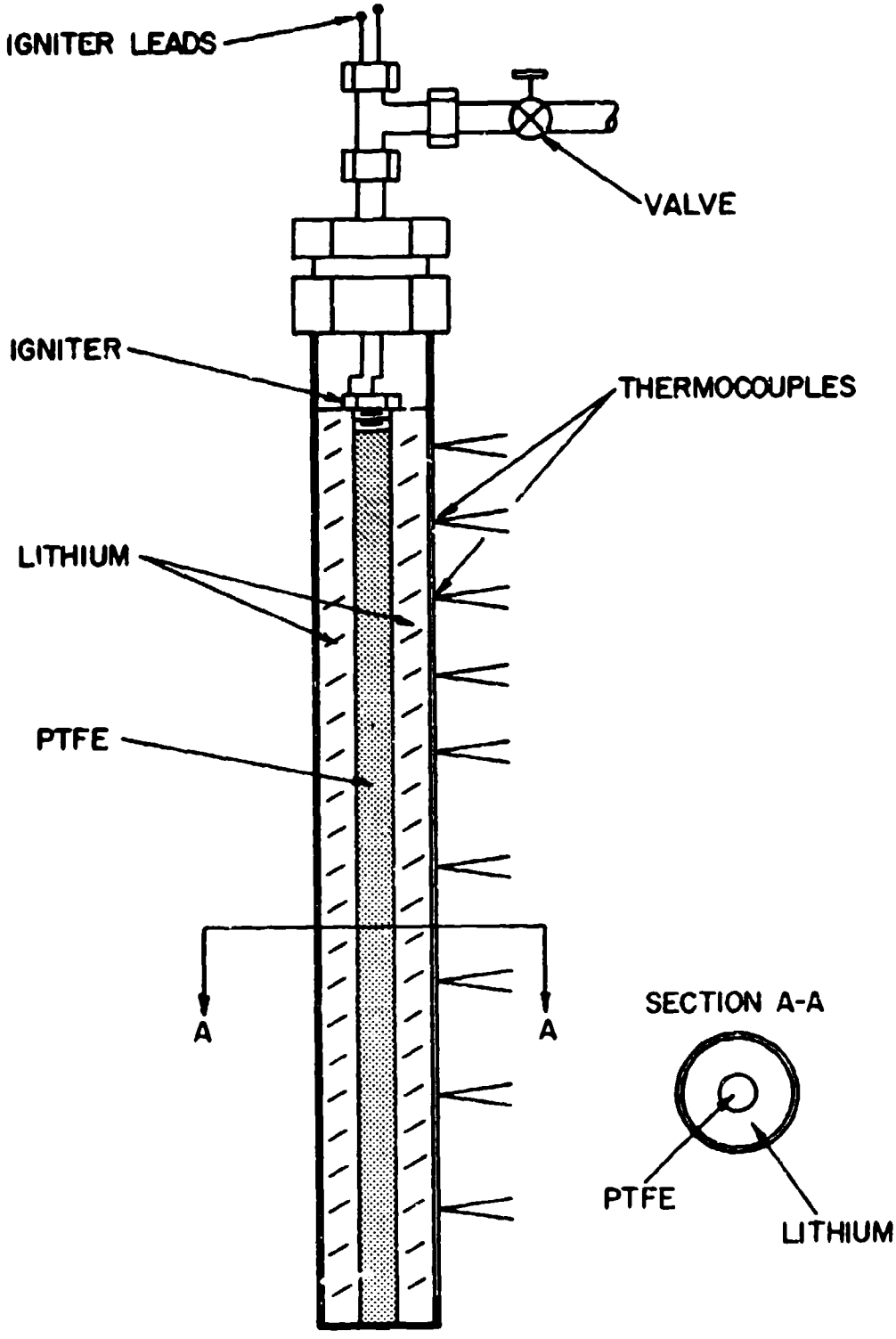

Figure 1 Preliminary Test Apparatus

was run, the device was evacuated and the valve was closed, isolating the system. The igniter was then fired, and the reaction was seen to traverse the length of the sample in approximately 0.035 seconds, corresponding to an average velocity of about 5.5 m/s. The arrival of the reaction front at each subsequent thermocouple location was evidenced by a sharp deflection on the corresponding analog output record, indicating a rapid increase in temperature at that point. Visual inspection of the apparatus and its contents after the test run indicated that all of the PTFE resin had been consumed in the reaction. In addition, no evidence of high pressure within the device was seen. It was, however, recognized that the placement of the thermocouples on the outside of the sample tube introduced a considerable time lag in the measuring system. It was, therefore, decided to carry out some more refined tests in an attempt to get some more basic information on the characteristics of this reaction.

The second series of test runs in the cylindrical configuration was carried out in an apparatus as shown in Figure 2. The sample tube was again of sufficient size to allow the insertion of a commercial 25.4 mm diameter x 203 mm lithium rod, and the hole into which the PTFE resin was placed was again created by forcing a length of tubing through the lithium sample. In this configuration, however, the igniter was threaded into a plug which was in turn welded into one end of the sample tube, and the closure at the opposite end of the tube was affected by a removable cap incorporating a redundant high temperature O-ring seal. This cap was held on during testing by a retainer ring and four tie bolts. The most important refinement included in this device was, however, the placement of the

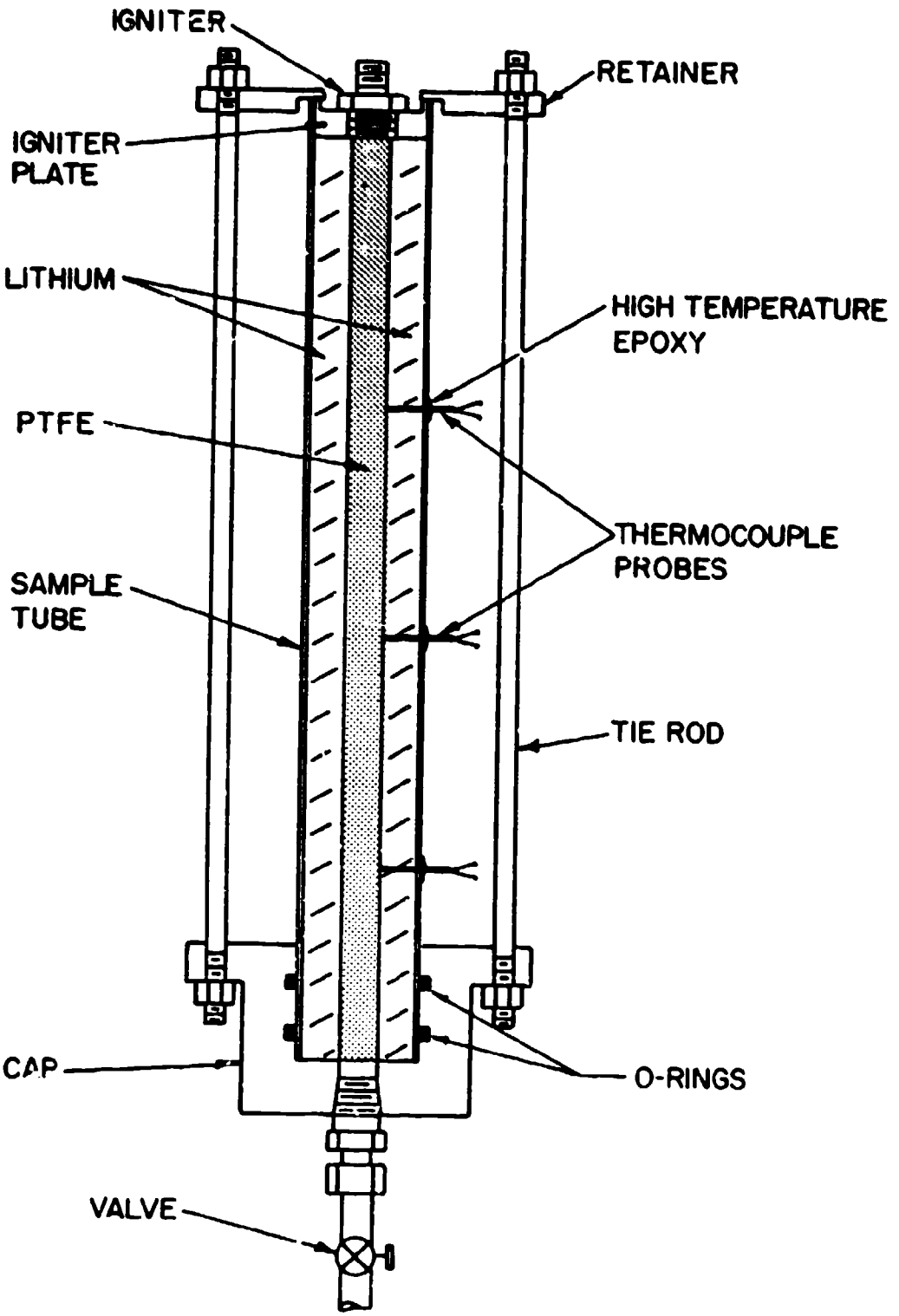

Figure 2 Improved Test Apparatus

thermocouple measuring junctions at the lithium-PTFE interface. This was accomplished through the use of fine wire (0.15 mm diameter) exposed junction thermocouple probes having a sheath diameter of 1.0 mm. The thermocouple probes were installed after the lithium rod was inserted and the hole for the PTFE resin was created. They were sealed at the surface of the sample tube with high temperature epoxy. After the thermocouple probes and the PTFE resin were in place and the cap and tie bolts secured, the thermocouple probes were connected to a recording oscillograph, and the device was evacuated in preparation for the firing of the igniter. During the period of time that the lithium was exposed to the air, the device was continuously bathed in argon gas in an attempt to minimize contamination of the specimen. A total of four successful preliminary tests were conducted with this apparatus. The nominal amounts of reactants involved were 50 g of lithium and 12 g of PTFE resin, and the average rate of propagation of the reaction front was 36.3 m/s with a range of 29 to 45 m/s. On additional test was conducted, in which the reaction was seen to propagate over approximately 10% of the length of the specimen and then stop. This was attributed to non-uniform packing of the PTFE resin.

From the results of these experiments in the cylindrical configuration, it was concluded that the chemical reaction between lithium and PTFE resin, each initially at room temperature and under a vacuum, was self-propagating when properly ignited, and was extraordinarily fast. It was therefore decided that a more thorough investigation into this reaction process should be undertaken,

although it was clear that the ignition of this reaction was a difficult task requiring an ignition source high in both quantity and rate of energy output.

1.2 Some Similar Reaction Studies Involving One or More Condensed Phases

The chemical reaction between lithium and PTFE, which is heterogeneous on both the macroscopic and the microscopic scale in the configuration utilized in the preliminary experiments described, is believed to follow the stoichiometry

$$6Li + C_2F_4 \rightarrow 4LiF + Li_2C_2 \quad . \qquad (1.1)$$

At room temperature, the reactants are in the solid phase, as are the products. An estimate of the adiabatic flame temperature of stoichiometric amounts of lithium and PTFE, based on currently available thermochemical information [1-3], indicated that this temperature was of the order of 2000 K, well above the melting point of standard materials of construction such as stainless steel. In order to preclude the melting of the sample container tube during testing, a quantity of lithium in excess of that required to combine stoichiometrically with the PTFE present was included. The overall reaction may thus be represented by

$$(6 + XS)\ Li + C_2F_4 \rightarrow 4LiF + Li_2C_2 + XS\ Li \quad , \qquad (1.2)$$

where:

XS = number of moles of lithium present in excess of that required by stoichiometry.

In the preliminary experiments, the amount of excess lithium was chosen such that the mean temperature of the reaction products and excess lithium immediately after the reaction had taken place was 1100-1150 K. The melting temperature of lithium fluoride is 1121 K [1]; lithium carbide does not melt but decomposes to graphite and lithium vapor at 1 atmosphere pressure at 1825 K [2]. The material within the sample container tube immediately after the reaction had occurred thus consisted of liquid lithium, solid or liquid LiF, and solid Li_2C_2.

A literature search was conducted on the subject of macroscopically heterogeneous chemical reactions in which condensed phase reactants form condensed phase products, from which no pertinent references were obtained. It was therefore decided that an examination of some previous reaction studies involving one or more condensed phases might prove instructive.

1.2.1 Lithium-Gas Surface Reactions

The chemical reaction between dry oxygen and a molten lithium surface was investigated by Tyzack and Longton [4] at subatmospheric pressures and at temperatures up to 1173 K. The primary purpose of this work was to measure the ignition temperature of the lithium-oxygen reaction as a function of oxygen pressure. The minimum ignition temperature observed was 900-920 K which occurred at pressures from 0.13 to 0.67 bar. Ignition temperatures as high as 1073 K were found at pressures above and below this range. Since the reaction product, lithium oxide, was in the solid phase at the temperatures encountered in the experiments, some reaction rate data was obtained by measuring

the change in the oxygen reservoir pressure as a function of time over a period of approximately 30 minutes following ignition. Only representative rate data were reported, and no estimates of activation energy or rate constant were presented. No analytical model was proposed.

Longton [5] studied the surface reaction between molten lithium and nitrogen over the pressure range 0.07-1.0 bar, and at temperatures from 573 to 723 K. From experiments similar to those of Tyzack and Longton [4], but with a typical time duration of 100 minutes, this reaction was found to follow a parabolic rate law after a short initial period. The activation energy was determined, and the rate constant was tabulated as a function of lithium temperature and nitrogen pressure. No analytical effort was reported.

Chandrasekharaiah and Margrave [6] conducted investigations of the oxidation and nitridation of a lithium surface. In this study, no oxidation rate measurements were made since the rates were found to be immeasurably small at low temperatures, and no containment material could be found which was suitable for use at high temperature. Nitridation rate measurements were made during 50 to 120 minute time periods following exposure of the metal to nitrogen gas at pressures of 0.15 and 0.27 bar. The metal surface temperatures during these experiments ranged from 512 to 583 K. The measured reaction rates were erratic and the apparent activation energy was reported to lie between 42 and 188 kJ/mole. No analytical model was postulated.

The nitridation of solid and molten lithium was studied by McFarlane and Tompkins [7] at temperatures from 273-638 K and at

pressures from 0.13-0.67 bar. The reaction rate of nitrogen with a solid lithium surface was observed to increase with time until the point at which a critical thickness of the lithium nitride reaction product had formed. Subsequent to the attainment of this critical thickness, the reaction rate was reported to be constant with time but pressure dependent A pressure-independent parabolic rate with 64.9 kJ/mole activation energy was observed for the surface reaction of nitrogen with molten lithium. Test data were obtained during periods of up to 200 minutes following exposure of the lithium to the nitrogen, and no analytical model was presented

The surface reaction of molten lithium with nitrogen and oxygen, as well as with the halogenated gases CCl_2F_2, C_4F_8 and SF_6 was investigated by Little [8]. Rate data were presented for the reaction of lithium with N_2, CCl_2F_2 and C_4F_8 at times from 0.5 to 300 seconds following exposure of the clean metal surface, at temperatures from 640 to 1000 K, to the reactant gas at pressures from 0.001 to 0.1 bar. The reaction rate between lithium and nitrogen was reported to be pressure-independent while the rates of the reactions of lithium with both CCl_2F_2 and C_4F_8 were observed to depend on the gas pressure. The ignition temperature of the lithium oxygen reaction was reported to be 880 K, and the lithium-SF_6 reaction was observed to ignite at 1063 K, corresponding to the temperature at which the reaction products become liquid. A criterion for the occurrence of a surface reaction was developed, but no analytical reaction rate model was presented.

1.2.2 Composite Solid Propellant Combustion

Composite solid propellants are plastic-like materials consisting of small oxidizer particles embedded in a fuel matrix. Ammonium perchlorate is the most commonly used oxidizer, and the fuel, which also acts as a binder, is generally a plastic or rubber material. Composite solid propellants are therefore homogeneous on the macroscopic scale, but microscopically heterogeneous. Typical experimental investigations [9] involve the burning of the propellant at constant pressure over the range 7-200 bar. The products of combustion are gaseous. Linear self-propagating burning rates of the order of 10-100 mm/s are found to be a function of propellant composition and particle size, environmental pressure, propellant temperature, and the nature of the gas flow relative to the burning surface. The actual combustion process is very complex, with endothermic decomposition reactions supplying gaseous fuel and oxidizer which subsequently participate in one or more exothermic chemical reactions.

The earliest analytical treatment of composite solid propellant combustion is the "Granular Diffusion Flame" model of Summerfield, et al., [10]. Through a primarily qualitative line of reasoning, the authors were able to produce a relationship between the linear burning rate and the environmental pressure. Fenn's "Phalanx Flame" model [11], which is also qualitative in nature, predicts a similar burning rate-pressure relationship through a different set of arguments. Both the Summerfield, et al., [10], and the Fenn [11] models are essentially heuristic devices, intended

to provide some physical insight into the phenomena occurring, and to serve as a starting point for the development of more complete theories. More rigorous analytical treatments by Hermance [12], and Culick and Dehority [13] have also been reported, but as yet no widely accepted comprehensive theory of the combustion of composite solid propellants exists.

1.2.3 Flame Spread Over the Surface of Condensed Phase Materials

An understanding of the mechanism by which a flame spreads over the surface of a solid or liquid material in an oxidizing gaseous environment is of major importance in such areas of interest as the ignition of solid propellant rocket motors and the advance of forest fires. In the case in which the surface of a solid is involved, the flame spreading velocity has been found experimentally [14-20] to be effected by the chemical composition and surface texture of the condensed-phase material, the details of the movement (if any) of the gaseous environment, the orientation and geometry of the surface, the thickness of the fuel mass, the ambient oxidizer concentration, and the total ambient pressure. Analytical models of the spread of a flame over a solid surface differ chiefly in the assumptions made relative to the dominant mode of heat transfer from the advancing flame forward to preheat and vaporize the unburned surface.

McAlevy and Magee [21] postulated that the flame spreading velocity is controlled by the gas-phase heat and mass transfer occurring within a small "ignition region" immediately ahead of the flame. Through a simplified analytical treatment and the use of

experimentally-determined temperature profiles, the authors arrived at a power-law relationship between the total pressure, the oxidizer mole fraction, and the flame spreading velocity which was seen to correlate experimental data with a reasonable degree of success. Solid-phase phenomena were ignored. In a later effort by Lastrina, Magee, and McAlevy [22], both gas and solid-phase analyses were included. Flame spreading velocity control by the processes taking place within the ignition region was again postulated, but differences in these controlling processes caused by the fuel being thermally "thick" (temperature gradients within the fuel in the direction normal to the surface are non-negligible), or thermally "thin" (temperature of the fuel is constant in the direction normal to the surface) were taken into account. Simple algebraic equations of the power-law type for the flame spreading velocity over thermally thick and thermally thin fuel beds resulted. These relations, although requiring experimental information in order to be evaluated, have been used quite successfully by the authors to correlate experimental results.

Flame spreading over both thermally thick and thermally thin solid fuel beds has also been treated analytically by de Ris [23]. It was assumed that the heat transfer from the flame forward to the unburned fuel was by solid and gas-phase conduction in the case of the thermally thick-fuel, and by gas-phase conduction only in the thermally thin situation. By the choice not to identify a finite ignition region, and the assumption of infinite reaction rates, the model was made amenable to treatment by diffusion flame theory, and an exact mathematical solution was possible. The

resulting expressions for the flame spreading velocity, which also require the input of experimental data in order to be evaluated, have been shown to be similar [15] to those developed by Lastrina, Magee, and McAlevy [22] for fuel beds of like thermal thickness. This similarity is surprising in light of the considerable difference in assumptions regarding the existence of the finite ignition region.

Another model of the process of flame spreading over solid surfaces, in which radiation is assumed to be the dominant mode of heat transfer from the flame to the unburned fuel, has been proposed by Tarifa, Notario, and Torralbo [24]. By ignoring conduction and convection of energy, a consideration of the effects of the thermal thickness of the fuel bed was made unnecessary. The resulting implicit expressions involving the flame spreading velocity are sufficiently complex as to preclude quantitative comparison with experimental results.

Heat conduction forward through the solid fuel bed is assumed to be the major mode of heat transfer in an additional model proposed by Fernandez-Pello and Williams [17]. This model was specifically constructed for the spread of a laminar flame over the surface of polymethylmethacrylate (PMMA), and an analytical expression for the flame spreading velocity involving one empirical constant was produced. Agreement with experimental observation is quite good, although the authors caution the use of this model to predict flame spreading velocities for situations in which the fuel is other than PMMA.

Finally, Feng and Sirignano [25] have analytically treated the process of flame spreading over the surface of materials which

undergo an exothermic surface reaction. Effects of fuel bed thickness and motion of the gaseous environment on the flame spreading velocity were considered; conduction through the solid was assumed to be the dominant heat transfer mode. However, since the exothermic reaction occurring in the combustion of the materials studied experimentally [14-20] is not a surface reaction but rather takes place in the gas phase, a meaningful comparison of the predictions of this model with experimental observation was precluded.

In the case of flame spread over the surface of a liquid below its flash point, the flame spreading velocity has been observed to be controlled by the flow of the liquid caused by surface tension and buoyancy effects. The occurrence of this liquid flow phenomenon has been pointed out by the work summarized in a paper by Akita [26], and by a more recent experimental study by Helmstetter, Dryer, and Glassman [27]. Thus, an additional level of complexity is present over the case in which the fuel is a solid, and attempts at analysis to date have met with only limited success. It is interesting to note that several of the analytical efforts previously discussed on the flame spread over solid surfaces [21, 23, 24] originally purported to be applicable to liquid surfaces as well. However, the phenomenon of liquid flow during the flame spreading process was not considered in these models, and the results are therefore not germane in this situation.

1.2.4 Exothermic Alloying of Metals

In the process in which metals are alloyed to produce enhanced physical properties or reduced cost, a knowledge of the

time required for the alloying reaction to take place is of great importance. This fact has prompted several studies (e.g., 28, 29, 30) of the rates of formation of various alloys. The particular situation in which the alloying reaction is exothermic and self-propagating has been investigated analytically by Hardt and Phung [31], and experimentally by Hardt and Holsinger [32]. Self-propagating reactions were found to take place only in cases in which the reaction products were liquids. A model based on a mass diffusion-controlled, condensed phase exothermic chemical reaction occurring in "diffusion cells" of linear geometry was developed, and the resulting set of equations was solved numerically in dimensionless form. A highly simplified explicit solution was also presented. Reasonable agreement between analytical prediction and experimental measurement of reaction propagation velocities was obtained.

1.2.5 Combustion of Magnesium-PTFE Pyrotechnic Pellets

In view of a relatively high energy density, and the fact that the products of combustion are condensable, magnesium-PTFE pyrotechnic pellets have seen increasing use in recent years as ignition materials for use in solid propellant rocket engines and similar applications. Fabricated by compressing a mixture of very small magnesium particles and PTFE resin, these macroscopically homogeneous pellets are available commercially in a variety of sizes and shapes [33]. In the only work reported in the literature, Griffiths, O'Sullivan, and Thackery [34] investigated flame shapes, flame spectra, and burning times during the lengthwise combustion

of cylindrical magnesium-PTFE pellets at constant pressure over the range 0.02-1.0 bar. Pellets containing 30 to 60 weight percent magnesium were studied, the stoichiometric composition being 32 weight percent magnesium, as given by the overall combustion reaction

$$Mg + \frac{1}{2} C_2F_4 \rightarrow MgF_2 + C \quad , \tag{1.3}$$

which was confirmed by calorimetry. The flame was observed to be a thin disc located on the burning surface of the pellet during combustion at 1.0 bar; at lower pressures, this zone was seen to expand and move away from the pellet surface. S-shaped pressure versus burning time curves were reported for pellets containing 50 weight percent magnesium, from which the authors postulated the existence of two burning regimes. In both cases, the burning rate is assumed to be controlled by the rate at which the solid PTFE is thermally decomposed to gaseous C_2F_4, which then reacts with the magnesium. In the high pressure burning regime, it is proposed that the heat required to thermally decompose the PTFE comes from the flame, while at lower pressures, it is felt that this heat comes from an exothermic surface reaction. No analytical model of the actual combustion process was, however, presented.

1.3 Specific Research Objectives

In light of the promising results from the preliminary experiments previously described, the chemical reaction of lithium with PTFE appeared as an interesting and viable high energy density heat source. However, no previous work directly applicable to this system, either of an analytical or an experimental nature, was

reported. In order to gain more insight into the lithium-PTFE reaction process, then, further work was indicated. The specific objectives of this investigation are, therefore, as follows:

1. To design and construct an apparatus with which the lithium-PTFE reaction propagation process might be experimentally examined.
2. To conduct an experimental investigation of the influence of varying the diameter and density of PTFE on the reaction propagation velocity.
3. To develop a model for the lithium-PTFE reaction propagation process.

CHAPTER II

THEORETICAL CONSIDERATIONS

2.1 Description of the Proposed Reaction Mechanism

Thermochemical calculations previously described have indicated that the products of the lithium-PTFE reaction, under the conditions of interest, are in the condensed phase. Supporting evidence for this conclusion may be found in the results of the preliminary experiments described in Section 1.1, in which no indication of high pressure within the sample container tube, after the reaction had taken place, was seen. Further, if it is assumed that the reaction products are, indeed, gaseous, and that they are forced to occupy the same volume as originally taken up by the reactants, as necessarily must be the case in a sample container with minimal free volume, a perfect-gas law estimation of the pressure required to achieve the dictated density at reasonable temperatures indicates that a pressure level of the order of 3500 bar is necessary. Since the existence of a pressure of this order of magnitude would surely have manifested itself in the experiments by deformation or rupture of the sample container tube, it is concluded that the products of the lithium-PTFE reaction are, in fact, in the condensed phase as originally postulated The answer to this important question having been satisfactorily ascertained, the following mechanism for the lithium-PTFE reaction process is proposed:

The overall reaction rate-controlling process is assumed to be the thermal decomposition of PTFE, as set forth by Griffiths,

et al., [34] for the combustion of magnesium-PTFE pyrotechnic pellets. It is postulated that the PTFE decomposes to give the gaseous monomer C_2F_4, found to be the predominant decomposition product in vacuum pyrolysis studies [35-37], according to an Arrhenius-type first-order rate law obtained from vacuum pyrolysis data [37, 38]. This C_2F_4 gas is assumed to chemically react immediately upon its formation with liquid lithium to form condensed-phase products according to the combustion reaction previously set forth

$$6Li + C_2F_4 \rightarrow 4LiF + Li_2C_2 \qquad (1.1)$$

Heat transfer from the reacting lithium and C_2F_4 forward to preheat and thermally decompose the unreacted PTFE is assumed to occur only by condensed-phase conduction, and it is by the rate at which this heat transfer takes place that the reaction propagation velocity is controlled.

2.2 One-Dimensional Model

At the outset of the analytical phase of this work, it was decided that a preliminary investigation of the lithium-PTFE reaction process at the one-dimensional level might prove instructive. It was felt that even though many of the intuitively important aspects of this process would be ignored by necessity in a one-dimensional description, an indication of the validity of the pivotally important assumptions which were made relative to the identity of the overall reaction rate-controlling process and the predominant mode of heat transfer would be gained. Accordingly, the one-dimensional, constant property form of the heat conduction equation with heat

generation [39],

$$\frac{\partial T}{\partial t} = \alpha \frac{\partial^2 T}{\partial x^2} + \frac{\dot{q}}{\rho C_p} \qquad (2.1)$$

was solved numerically in dimensional form. Stoichiometric mixtures of lithium and PTFE only were considered, the presence of lithium in excess of the stoichiometric amount and the accompanying loss of heat to this excess lithium being ignored. The rate of heat generation was assumed to be determined by the rate of thermal decomposition of the PTFE, and the conduction of heat through the PTFE was considered negligible. Although several additional highly unrealistic assumptions were necessarily made out of deference to the desire for a one-dimensional representation, the predicted reaction propagation velocity was approximately 240 m/s, which is of the same order of magnitude as the reaction propagation velocities measured in preliminary experiments. The fact that the predicted velocity was of the correct order of magnitude was considered highly encouraging. It was felt that the two-dimensional effects to be included in subsequent models would produce a decrease in the predicted reaction propagation velocity, bringing it into better agreement with experimental observations.

2.3 Two-Dimensional Model

The two-dimensional model of the lithium-PTFE reaction process is shown schematically in Figure 3. As seen in this sketch, the model is in cartesian coordinates, with a layer of PTFE of thickness h_T located adjacent to a layer of lithium of total thickness h_L. The amount of lithium required to react stoichiometrically

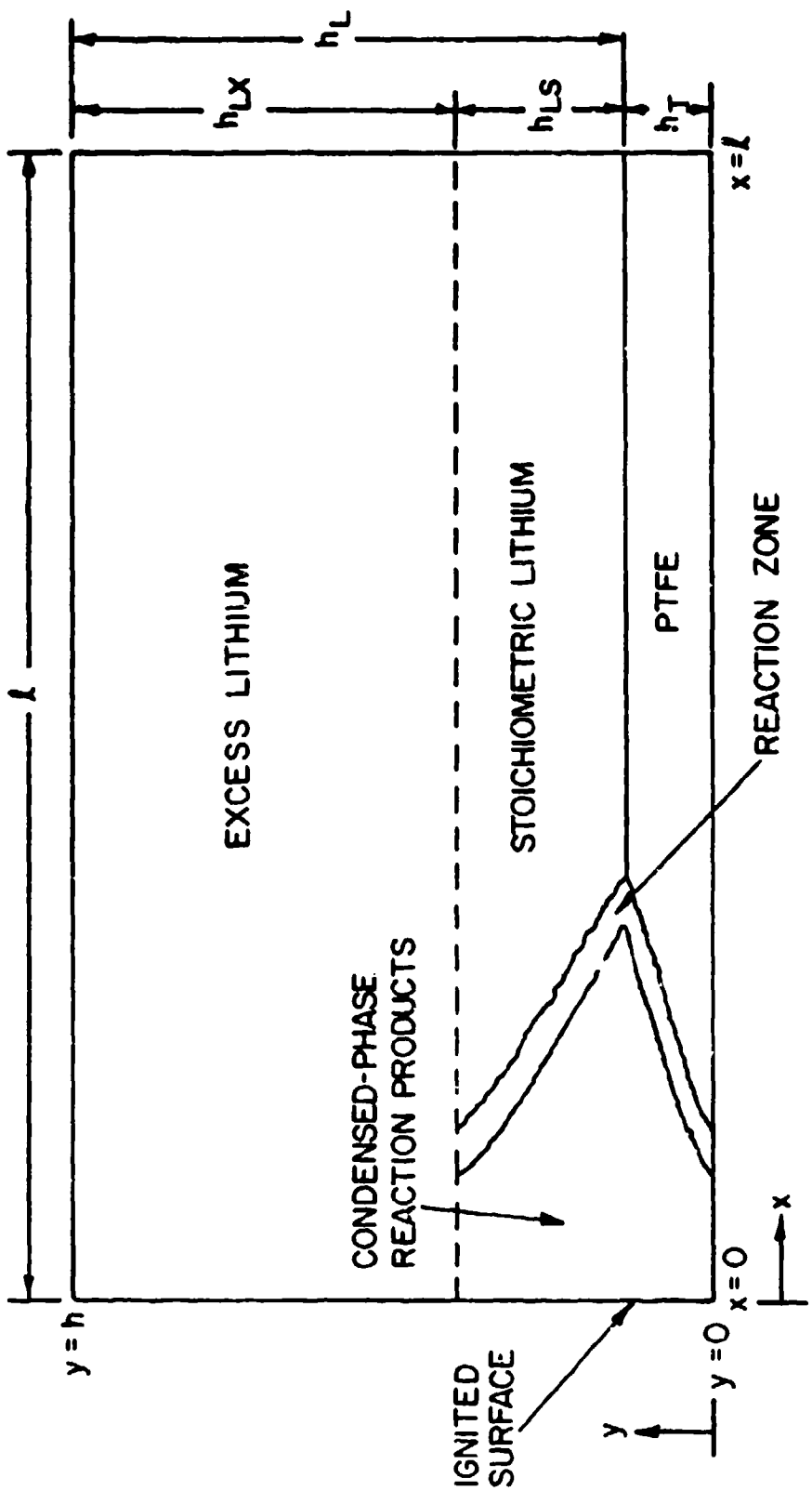

Figure 3 Lithium-PTFE Reaction Model

with the PTFE is of thickness h_{LS}, the excess lithium layer is of thickness h_{LX}, and the length of the sample is ℓ. The reaction zone, which moves from left to right, contains unreacted lithium, unreacted PTFE, and reaction products. Heat generated within the reaction zone is transferred by conduction to the lithium, to the PTFE, and to the reaction products. As shown in Figure 3, the reaction products are assumed to be in the condensed phase, and to occupy the volume originally taken up by the PTFE and the stoichiometric lithium. The lithium-PTFE reaction process is assumed to be initiated by the action of an ignition source, which serves to start the chemical reaction of a small amount of lithium and PTFE located at the x=0 end of the sample adjacent to the lithium-PTFE interface, and to maintain the reaction products produced at this location at the stoichiometric adiabatic flame temperature. It is further assumed that there are no external heat losses from the sample.

Since the overall reaction rate is assumed to be controlled by the rate of thermal decomposition of the PTFE, it is therefore postulated that the reaction actually occurs at the decomposing surface of the PTFE. For this region, the two-dimensional constant property form of the heat conduction equation with heat generation [39],

$$\frac{\partial T}{\partial t} = \alpha\left(\frac{\partial^2 T}{\partial x^2} + \frac{\partial^2 T}{\partial y^2}\right) + \frac{q}{\rho C_p} \quad , \tag{2.2}$$

may be written. In the stoichiometric lithium layer and in the excess lithium layer, where no reaction is assumed to take place, the temperature field may be described by the following equation [39]:

$$\frac{\partial T}{\partial t} = \alpha \left(\frac{\partial^2 T}{\partial x^2} + \frac{\partial^2 T}{\partial y^2} \right) \quad , \tag{2.3}$$

which is identical to Equation (2.2) with the exception that no heat source term is present. Although constant property forms of the heat conduction equation have been written, it is recognized that the thermal diffusivity, α, in the above two equations is not constant, but rather is a function of the mass fractions of reactants and products present in the PTFE and the stoichiometric lithium layers. This fact will be accounted for in the subsequent solution of these equations.

In order to arrive at an expression for the rate of heat generation per unit volume, $\dot{q}$, occurring in the PTFE layer, attention is focused on the Arrhenius-type first-order rate equation for the vacuum pyrolysis of PTFE [37],

$$\frac{dm}{dt} = -A_o m e^{-E_a/RT} \quad , \tag{2.4}$$

where:

m = undecomposed mass of PTFE.

The mass fraction of undecomposed PTFE, Z_T^*, is now defined as follows:

$$Z_T^* = \frac{m}{m_o} \quad , \tag{2.5}$$

where:

m_o = original mass of PTFE.

Substitution of Equation (2.5) into Equation (2.4) and cancellation of common terms yields:

$$\frac{dZ_T^*}{dt} = -A_o Z_T^* e^{-E_a/RT} \quad . \tag{2.6}$$

An expression for the heat generation per unit volume occurring in the PTFE layer may then be written as follows:

$$\dot{q} = -(\rho_T \Delta H_R W) \frac{dZ_T^*}{dt} \quad , \tag{2.7}$$

the negative sign arising since the rate of heat generation is proportionaly to the rate of evolution of C_2F_4 vapor, which is numerically equal to the rate of decrease of the mass of undecomposed PTFE, but of opposite sign.

The two-dimensional analytical model for the lithium-PTFE reaction process therefore consists of the following set of equations:

In the PTFE:

$$\frac{\partial T}{\partial t} = \alpha\left(\frac{\partial^2 T}{\partial x^2} + \frac{\partial^2 T}{\partial y^2}\right) - \left(\frac{\rho_T \Delta H_R W}{\rho C_p}\right)\frac{dZ_T^*}{dt} \quad , \tag{2.8}$$

where:

$$\frac{dZ_T^*}{dt} = -A_o Z_T^* e^{-E_a/RT} \quad . \tag{2.6}$$

In the stoichiometric and excess lithium:

$$\frac{\partial T}{\partial t} = \alpha\left(\frac{\partial^2 T}{\partial x^2} + \frac{\partial^2 T}{\partial y^2}\right) \quad . \tag{2.3}$$

The appropriate boundary and initial conditions are as follows:

Boundary Conditions:

$$x = 0,\ y \neq h_T\ ;\quad \frac{\partial T}{\partial x} = 0$$

$$x = 0,\ y = h_T\ ;\quad T = T_{af}\ ,$$

$$x = \ell\ ;\quad \frac{\partial T}{\partial x} = 0\ ,$$

$$y = 0\ ;\quad \frac{\partial T}{\partial y} = 0\ ,$$

$$y = h\ ;\quad \frac{\partial T}{\partial y} = 0\ . \tag{2.9}$$

Initial Conditions:

$$t = 0\ ;\ T = To\ ,\ \text{all } x, y, \text{ except}$$

$$t = 0\ ;\ T = T_{af}\ ,\ x = 0,\ y = h_T\ ,$$

$$t = 0\ ;\ Z_T^* = 1\ . \tag{2.10}$$

In order to make the model more general, and to reduce the number of parameters which characterize the system, the following dimensionless variables are defined:

$$X^* = \frac{x}{\sqrt{\alpha_T t_{ch}}}\ ,$$

$$Y^* = \frac{y}{\sqrt{\alpha_T t_{ch}}}\ ,$$

$$\tau^* = \frac{t}{t_{ch}}\ ,$$

$$T^* = \frac{T}{T_{af}}\ , \tag{2.11}$$

where:

T_{af} = the stoichiometric adiabatic flame temperature at one atmosphere total pressure

and

t_{ch} = the time required to thermally decompose an arbitrary fraction of an amount of PTFE at this stoichiometric adiabatic flame temperature.

Substituting these dimensionless variables into Equations (2.3), (2.7), and (2.8) yields:

In the PTFE:

$$\frac{\partial T^*}{\partial \tau^*} = \frac{\alpha}{\alpha_T}\left(\frac{\partial^2 T^*}{\partial X^{*2}} + \frac{\partial^2 T^*}{\partial Y^{*2}}\right) - \left(\frac{\rho_T \Delta H_R W}{\rho C_P T_{af}}\right)\frac{dZ_T^*}{d\tau^*} \quad , \tag{2.12}$$

$$\frac{dZ_T^*}{d\tau^*} = -(A_o t_{ch})\, Z_T^* e^{-(E_a/RT_{af})\frac{1}{T^*}} \quad . \tag{2.13}$$

In the stoichiometric and excess lithium:

$$\frac{\partial T^*}{\partial \tau^*} = \frac{\alpha}{\alpha_T}\left(\frac{\partial^2 T^*}{\partial X^{*2}} + \frac{\partial^2 T^*}{\partial Y^{*2}}\right) \quad . \tag{2.14}$$

The following dimensionless parameters are now defined:

$$A^* = \frac{\alpha}{\alpha_T} \quad ,$$

$$R^* = \frac{\rho_T \Delta H_R W}{\rho C_P T_{af}} \quad ,$$

$$F^* = A_o t_{ch}$$

$$E^* = \frac{E_a}{RT_{af}} \quad . \tag{2.15}$$

The parameters F* and E* above are constants. The parameter A* is in effect a variable, its value depending, first, on whether it is evaluated in the stoichiometric lithium layer or in the PTFE layer, and second, on the mass fractions of reactants and products present at the location in equation. Similarly, the value of the parameter R*, which pertains only to the PTFE layer, is a function of the chemical composition.

The dimensionless analytical model is then given by the following set of equations with appropriate boundary and initial conditions:

In the PTFE:

$$\frac{\partial T^*}{\partial \tau^*} = A^*\left(\frac{\partial^2 T^*}{\partial X^{*2}} + \frac{\partial^2 T^*}{\partial Y^{*2}}\right) - R^* \frac{dZ_T^*}{d\tau^*} , \tag{2.16}$$

$$\frac{dZ_T^*}{d\tau^*} = -F^* Z_T^* e^{-E^*/T^*} . \tag{2.17}$$

In the stoichiometric and excess lithium:

$$\frac{\partial T^*}{\partial \tau^*} = A^*\left(\frac{\partial^2 T^*}{\partial X^{*2}} + \frac{\partial^2 T^*}{\partial Y^{*2}}\right) . \tag{2.18}$$

Boundary Conditions:

$$X^* = 0 , \; Y^* < H_T^* \; ; \; \frac{\partial T^*}{\partial X^*} = 0 ,$$

$$X^* = 0 , \; Y^* = H_T^* \; ; \; T^* = 1 ,$$

$$X^* = L^* \; ; \; \frac{\partial T^*}{\partial X^*} = 0 ,$$

$$Y^* = 0 \; ; \; \frac{\partial T^*}{\partial Y^*} = 0 ,$$

$$Y^* = H^* \; ; \; \frac{\partial T^*}{\partial Y^*} = 0 \tag{2.19}$$

Initial Conditions:

$$\tau^* = 0 \quad ; \quad T^* = T_o^* \text{ , all } X^*, Y^*, \text{ except}$$

$$\tau^* = 0 \quad ; \quad T^* = 1 \quad , X^* = 0, Y^* = H_T^* \quad ,$$

$$\tau^* = 0 \quad ; \quad Z_T^* = 1 \quad . \tag{2.20}$$

2.4 Details of the Numerical Solution

As a first step in the numerical solution of the two-dimensional model, attention was focused upon the dimensional form of this model, as given by Equations (2.3), (2.6), (2.8), (2.9) and (2.10). The partial differential equations were cast into finite difference form, and a digital computer program for the numerical solution of the model was written. The purpose of this effort was to ascertain whether the predicted reaction propagation velocities were of reasonable magnitude, and to identify the variables to which the reaction propagation velocity was most sensitive. The particular techniques used in this numerical solution were identical to those used in the solution of the dimensionless form of the two-dimensional model, which will be described subsequently. The validity of the numerical solution of the partial differential equations was checked by comparison, under appropriate boundary conditions and with no heat generation, with the analytical solution for the transient heating of a semi-infinite slab [39], and was found to agree to within 0.5 percent. The numerical solution of the ordinary differential equation under the condition of constant temperature was compared with its analytical solution with similar results. For conditions similar to those present in preliminary experiments, the predicted reaction

propagation velocities were approximately 15% higher than those observed, which was considered to be reasonable agreement. Further, through a systematic variation of parameters, it was discovered that the reaction propagation velocity was most sensitive to small changes in the thermal diffusivity of the PTFE, α_T, and in the activation energy for the thermal decomposition of the PTFE, E_a. These results, then, provided the clue for the characteristic time and length scales of the system, which were used as normalizing parameters in the nondimensionalization of the model as given by Equation (2.11).

The dimensionless form of the two-dimensional model, as given by Equations (2.16-2.20), was then considered. The lithium-PTFE reaction sample was first broken up into a grid network as shown in Figure 4. As seen in Figure 4, the X* direction grid spacing, ΔX^*, was the same for the PTFE layer as for the stoichiometric and excess lithium layers. For the two lithium layers, the Y* direction grid spacing, ΔY_L^*, was also the same. The Y* direction grid spacing in the PTFE layer, ΔY_T^*, was however adjusted such that the amount of PTFE represented by each grid point in this layer was just that amount necessary to react stoichiometrically with the amount of lithium represented by each grid point in the stoichiometric lithium layer. The Y* direction grid spacing spanning the lithium-PTFE interface, ΔY_{LT}^*, was therefore equal to the average of ΔY_L^* and ΔY_T^*. The number of grid points in the PTFE layer was thus equal to the number of grid points in the stoichiometric lithium layer; the number of grid points in the excess lithium layer was arbitrary, but, once chosen, determined the amount of excess lithium present. The two heat

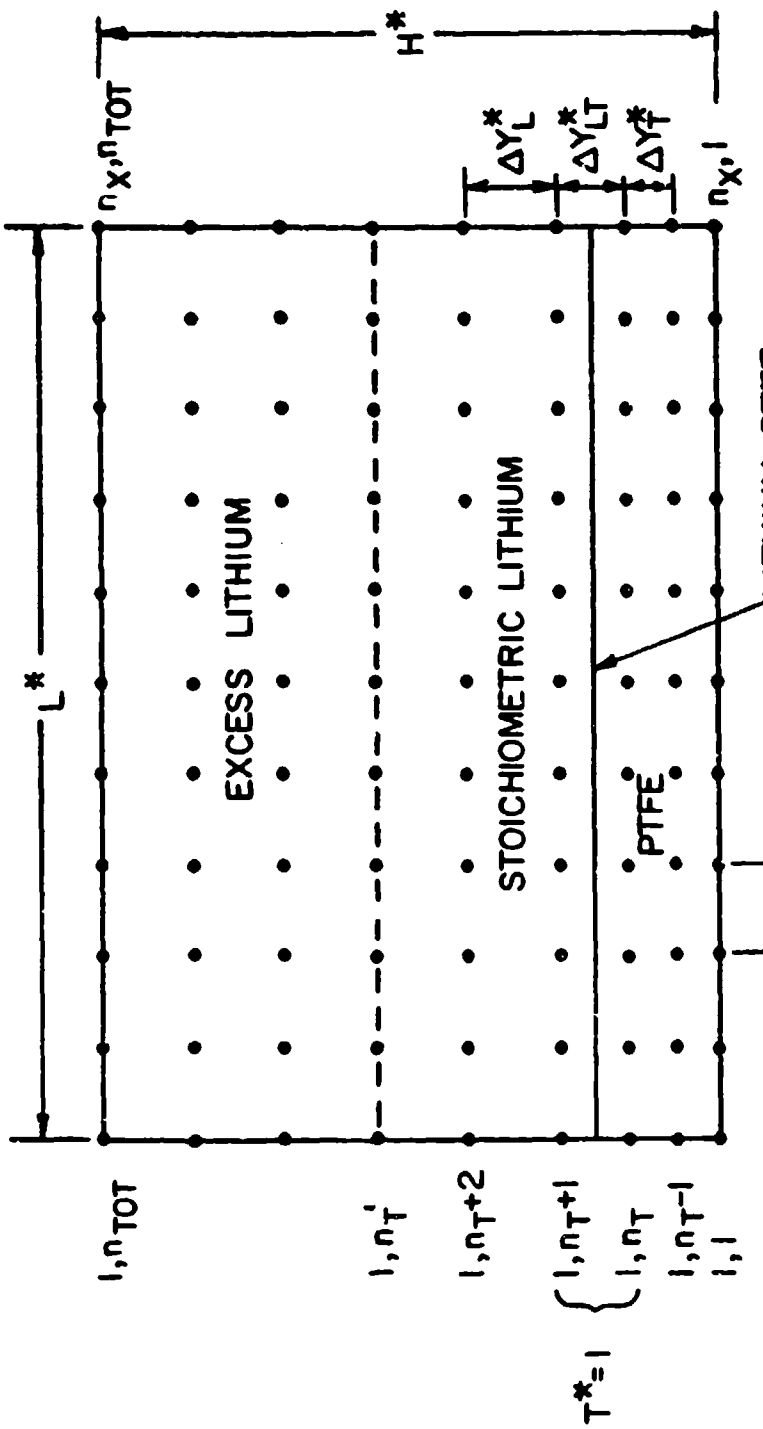

Figure 4 Sketch of Finite Difference Grid Network

conduction equations, Equations (2.16) and (2.18) were cast in finite difference form using the central difference approximation for the spatial derivatives and the forward difference approximation for the time derivatives [40]; the detailed nodal equations are presented in Appendix A. The ordinary differential equation, Equation (2.17) was put into form for numerical integration through the use of Euler's method [41].

For the purposes of the numerical solution of the model, it was assumed that the chemical reaction between the PTFE and the stoichiometric lithium took place according to the following sequence: As seen in Figure 4, the initial conditions given by Equation (2.20) dictated that reaction products at $T^*=1$ were present at grid points 1, n_T, and 1, n_T+1. The reaction zone was allowed to propagate along the lithium-PTFE interface at a rate determined by heat transfer and PTFE decomposition kinetics, the PTFE represented by grid points i, n_T reacting stoichiometrically with the lithium represented by grid points i, n_T+1. As the reaction zone spread into the PTFE and the stoichiometric lithium in the direction perpendicular to the lithium-PTFE interface, it was assumed that the PTFE represented by grid points i, n_T-1 reacted with the lithium represented by grid points i, n_T+2. This lateral spreading of the reaction zone was allowed to continue in this symmetrical manner through as many grid points as were located in the PTFE and stoichiometric lithium until the PTFE represented by grid points i, 1 had reacted with the lithium represented by grid points i, n_T'. At any given X^* location (any value of i between 1 and n_X), the reaction was required to have gone to completion at the pair of

reacting grid points closest to the lithium-PTFE interface before it was allowed to progress to the subsequent reacting grid point pair.

For the purpose of property computations, it was necessary to monitor the mass fractions of unreacted (undecomposed) PTFE and reaction products, and unreacted lithium and reaction products present in the PTFE and the stoichiometric lithium layers, respectively, as a function of dimensionless time. Initially, the mass fraction of unreacted PTFE, Z_T^*, at each of the grid points in the PTFE layer, with the exception of grid point 1, n_T, was unity and the reaction product mass fraction, Z_P^*, was zero. Similarly, the initial mass fraction of unreacted lithium, Z_L^*, was unity and the reaction product mass fraction, Z_P^*, was zero at each of the grid points in the stoichiometric lithium layer except at the grid point 1, n_T+1. As the PTFE was decomposed and reacted at each of the grid points in the PTFE layer, the value of Z_T^* at each point decreased according to Equation (2.17). The value of Z_L^* at each corresponding grid point in the stoichiometric lithium layer was therefore decreased as dictated by the assumed symmetrical nature of the lateral spread of the reaction zone. From this symmetry, and from the stoichiometric sizing of the grid network previously described, it is seen from Figure 4 that:

$$Z_L^*(i,\ 2n_T+1 - j) = Z_T^*(i,\ j) \tag{2.21}$$

and

$$Z_P^*(i,\ 2n_T+1 - j) = Z_P^*(i,\ j) = 1 - Z_T^*(i,\ j) \quad . \tag{2.22}$$

In order to accomplish the numerical solution of the dimensionless form of the two-dimensional model, it was necessary to compute the value of A*, the dimensionless thermal diffusivity ratio appearing in Equations (2.16) and (2.18). A knowledge of the thermal diffusivity, defined as

$$\alpha = \frac{k}{\rho C_p} \quad , \tag{2.23}$$

of the lithium, the PTFE, and the reaction products was therefore required. The values of the thermal conductivity, density, and specific heat used to determine the thermal diffusivities of the lithium and the PTFE were obtained from Reference [42], and Reference [43], respectively. The reaction products were assumed to possess the thermal conductivity [44], and the specific heat [1] of liquid lithium fluoride, which accounts for approximately 73 weight percent of the products according to the postulated reaction stoichiometry. The density of the reaction products was determined by the earlier assumption that these products are in the condensed phase, and fill the volume originally occupied by the unreacted lithium and PTFE.

The thermal diffusivity of all substances is a function of temperature, the value of α of pure lithium, for example, increasing by approximately a factor of 2 from the melting point to the normal boiling point [42]. However, during the course of the postulated reaction, in which the stoichiometric lithium and the PTFE are transformed into reaction products, the thermal diffusivity of the stoichiometric lithium is seen to decrease by a factor of 44, and that of the PTFE to increase by a factor of approximately 6.

For this reason, average values of the thermal conductivities, densities, and specific heats of the lithium, PTFE, and reaction products were used in the computation of the desired thermal diffusivity ratios, temperature variations in these ratios being neglected with respect to variations caused by changes in chemical composition.

In order to compute the value of the dimensionless parameter A* in the stoichiometric lithium layer as a function of chemical composition, the lithium and reaction products were assumed to form a perfect solution whose thermal conductivity, specific volume, and specific heat were linear functions of mass fraction. The thermal diffusivity ratio A* for this layer is, therefore, given by the following relationship:

$$A^* = \frac{\left(Z_L^* \frac{k_L}{k_T} + Z_P^* \frac{k_P}{k_T}\right)\left(Z_L^* \frac{\rho_T}{\rho_L} + Z_P^* \frac{\rho_T}{\rho_P}\right)}{\left(Z_L^* \frac{C_{P_L}}{C_{P_T}} + Z_P^* \frac{C_{P_P}}{C_{P_T}}\right)} \qquad (2.24)$$

The PTFE, however, was assumed to retain its original properties until completely reacted. As the reaction progressed at each grid point in the stoichiometric lithium layer, then, the value of A* was computed from Equation (2.24). At the corresponding grid point in the PTFE layer, the value of A* was held at unity until the reaction had gone to completion, at which time A* was set equal to that for the reaction products:

$$A^* = \frac{\alpha_P}{\alpha_T} \quad . \qquad (2.25)$$

Consistent with the assumption that the PTFE retained its original properties until reacted, the values for the density and specific heat of PTFE were used in the denominator of the dimensionless parameter R*, as given by Equation (2.15).

In order to simplify the numerical solution of the model, the melting processes occurring in the lithium and in the PTFE, and the heat absorbed in the vaporization of the PTFE were ignored. It was anticipated that erroneously high temperatures might be predicted by the numerical solution of the model as a result of neglecting these heat-absorbing phenomena, as well as from the use of average heat transfer properties as previously described. The predicted value of T* in the numerical solution was therefore limited to unity, corresponding to the assumption that the temperature at any point within the reaction sample could not exceed the stoichiometric adiabatic flame temperature for one atmosphere total pressure. Under actual experimental conditions, temperatures greater than the stoichiometric adiabatic flame temperature at standard conditions are possible due to the energy addition to the reaction sample caused by the firing of the igniter, and the lack of assurance that the reaction does not take place at pressures in excess of one atmosphere. However, in reality there are also heat losses from the sample, which have an opposing effect. In light of these facts, then, it is felt that this assumption is not unreasonable.

The nature of the solution of the PTFE thermal decomposition rate law, given in dimensionless form by Equation (2.17), is logarithmic, the value of Z_T^* approaching zero asymptotically. Since an infinite amount of dimensionless time would be required for the

undecomposed PTFE mass fraction to exactly go to zero, the chemical reaction at grid points in the PTFE layer was assumed to have gone to completion when the value of Z_T^* dropped below the value 0.10, corresponding to 90% of the PTFE having been decomposed and chemically reacted.

A digital computer program to accomplish the numerical solution of the dimensionless form of the two-dimensional model in the manner described above was written in Fortran IV language. A flow diagram of the computer program is presented in Appendix B. The numerical solution of the dimensionless heat conduction equations, Equations (2.16) and (2.18), with no heat generation and under appropriate boundary conditions, was again compared with the analytical solution for the transient heating of a semi-infinite slab [39], and was again found to agree to within 0.5 percent. The numerical solution of the dimensionless PTFE thermal decomposition rate equation, Equation (2.17), was also checked under constant temperature conditions with its closed-form solution with similar results. In addition, an energy balance check, in which the energy absorbed in the heating of the reactants and products was compared to the energy liberated by the chemical reaction, was incorporated into the computer program to insure that the numerical simulation was thermodynamically correct.

The dimensionless reaction propagation velocity was determined by continuously monitoring the product mass fraction at the grid points in the stoichiometric lithium and in the PTFE immediately adjacent to the lithium-PTFE interface. As the reaction zone moved along the lithium-PTFE interface and reaction was completed at each

successive pair of grid points adjacent to the interface, the dimensionless reaction propagation velocity was computed by dividing the dimensionless distance traversed, ΔX^*, by the dimensionless time elapsed since the previous pair of grid points had completely reacted. Examination of the dimensionless X^* and τ^* variables as given by Equation (2.11) then yields the following definition of the dimensionless reaction propagation velocity:

$$V^* = \frac{V}{V_{ch}} \quad , \tag{2.26}$$

where

$$V_{ch} = \sqrt{\frac{\alpha}{t_{ch}}} \tag{2.27}$$

2.5 Results of the Analytical Model

For the numerical solution of the dimensionless form of the two-dimensional model, the values of the thermal conductivity, density, and specific heat of the lithium were taken from Reference [42] as those for liquid lithium at 800 K. The properties of the PTFE were obtained from Reference [43], while the values of the frequency factor and the activation energy for the thermal decomposition of PTFE, as used in Equation (2.15), were taken from Reference [37]. The thermal conductivity and specific heat of the reaction products were obtained from Reference [44] and Reference [1], respectively, as those for liquid lithium fluoride at 1500 K, the density of the reaction products being determined as previously described. The values of the physical and chemical properties used in the numerical solution of the model are given in Appendix C

Using molecular weight data from Reference [1], the stoichiometric PTFE-lithium mass ratio was calculated from the assumed overall reaction mechanism, as given by Equation (1.1). The standard heat of formation of solid PTFE was determined by combining the standard heat of formation of gaseous C_2F_4 obtained from Reference [1] with the enthalpy of depolymerization of PTFE as given in Reference [37]. This quantity was then used in conjunction with additional data from Reference [1] to calculate the standard heat of reaction of lithium with PTFE, and the stoichiometric adiabatic flame temperature of this reaction at one atmosphere pressure. The stoichiometric adiabatic flame temperature under standard conditions was computed to be 1966 K, the normal boiling point of lithium fluoride, and the value of the characteristic time, t_{ch}, used as a normalizing parameter in Equation (2.11) was taken to be the time required to thermally decompose 90% of an initial amount of PTFE at this temperature.

The propagation of the reaction zone through the lithium-PTFE reaction sample, as predicted by the numerical solution of the model, occurs in the following manner: At the start of the solution, a period of time elapses during which no reaction occurs. In this "induction period," heat is conducted from the ignition source, located at the $X^*=0$ end of the sample at the lithium-PTFE interface, into the lithium and PTFE, preheating the reactants. Following this period, the reaction zone starts to move through the sample, experiencing an initial rapid acceleration. As the reaction zone approaches and passes through the center of the sample, the dimensionless reaction propagation velocity approaches a constant

value, this value rapidly increasing once again as the reaction zone nears the X*=L* end of the sample. For values of the dimensionless parameters A*, R*, F*, and E* determined as previously described, and a total PTFE to lithium mass ratio of 0.379, the predicted motion of the reaction zone is illustrated in Figure 5. In Figure 5, the dimensionless reaction propagation velocity V* is plotted as a function of dimensionless distance X* for two values of the dimensionless sample aspect ratio, L*/H*. As seen from this plot, the solutions are essentially identical up to the point X*=3.0. Beyond this point, the dimensionless reaction propagation velocity becomes more and more a function of L*/H*, indicating that the propagation of the reaction zone is strongly effected by the presence of the ends of the sample. At L*/H*=5, these end effects are quite pronounced, the value of V* increasing over the entire length of the sample. At L*/H*=10, however, the dimensionless reaction propagation velocity is seen to reach a level which is essentially constant over the central portion of the sample. Were it possible to increase the value of the dimensionless sample aspect ratio substantially, it is believed that the predicted dimensionless reaction propagation velocity would indeed reach a rigorously constant level. Computer storage capacity and run-time considerations, however, made this prohibitive.

One very important result of this analytical investigation was the prediction of the steady dimensionless reaction propagation velocity as a function of the total PTFE-lithium mass ratio. Based on the assumed overall combustion reaction given in Equation (1.1),

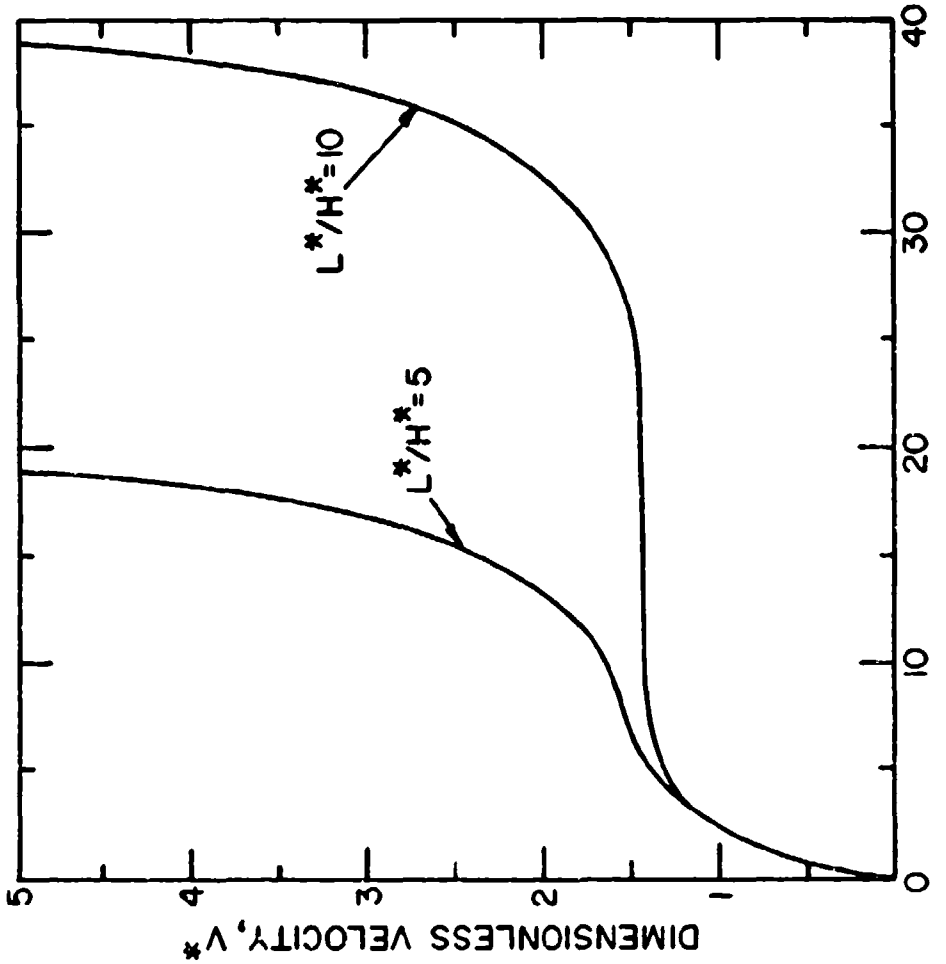

Figure 5 V* as a Function of X* for Two Values of L*/H* for PTFE-Lithium
Mass Ratio = 0.379

the stoichiometric PTFE-lithium mass ratio is 2.402. In order to limit the final equilibrium temperature of the material in the reaction sample, after the reaction had taken place, to a level below the melting point of standard materials of construction such as stainless steel, lithium in excess of that required to react stoichiometrically with the PTFE must be present. Based on the standard heat of formation of solid PTFE determined as previously described, and data from Reference [1], the dependence of the final equilibrium temperature on the PTFE-lithium mass ratio is shown in Figure 6. From Figure 6 it is seen that, in order to avoid excessive final equilibrium temperatures, a maximum PTFE-lithium mass ratio of approximately 0.4 is indicated, the discontinuity in this plot being due to the heat absorbed during the fusion of lithium fluoride at 1121 K. The lower limit of the PTFE lithium mass ratio range to be analytically investigated, as dictated by computer storage and run-time considerations, was 0.2, corresponding to a final equilibrium temperature of 980 K.

As seen in Figure 5, the dimensionless reaction propagation velocity does not, in fact, reach a truly steady level for either of the dimensionless sample aspect ratios examined, although the numerical solution for $L^*/H^*=10$ predicts a velocity which is very nearly steady. It was thus decided to investigate the variation in the dimensionless reaction propagation velocity, observed to be steady to within some tolerance level, as a function of total PTFE-lithium mass ratio for a dimensionless sample aspect ratio, L^*/H^*, of 10. The criterion for the selection of the steady value of V^* was taken to be the point at which the value of V^* was constant with X^* to within 1%. A

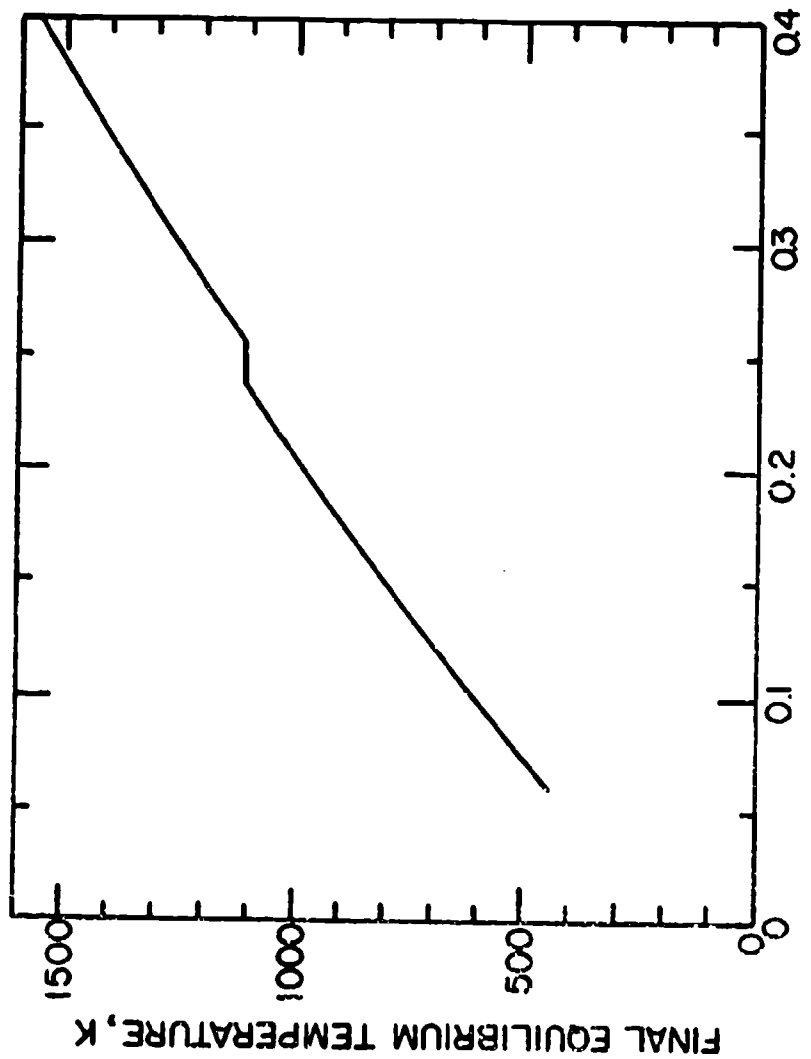

Figure 6 Final Equilibrium Temperature as a Function of PTFE-Lithium Mass Ratio

plot of the dimensionless steady reaction propagation velocity determined in this manner, V_S^*, as a function of the total PTFE-lithium mass ratio is shown in Figure 7. As seen from this plot, the value of V_S^* decreases linearly with increasing PTFE-lithium mass ratio over the range investigated. Over this range, the relationship between V_S^* and the PTFE-lithium mass ratio is:

$$V_S^* = 1.8575 - 1.1536\ M^* \quad , \tag{2.28}$$

where

M^* = PTFE-lithium mass ratio.

In order to illustrate the predicted dimensionless temperature profiles present in the reaction sample during the propagation of the reaction front, it was necessary to obtain a numerical solution of the model for a reaction sample with a small aspect ratio, L^*/H^*. This adjustment of the aspect ratio was required in order that the desired information could be represented with reasonable detail on a sketch of manageable physical size. The predicted dimensionless temperature profiles for a reaction sample with a value of L^*/H^* of 1.7, and a PTFE-lithium mass ratio of 0.206, are shown in Figure 8. In this sketch, the reaction front is seen to have moved approximately 1/3 of the distance through the sample, the dimensionless reaction propagation velocity at this point being constant with X^* to within 2.5%. In Figure 8, the $T^*=1$ isotherm present at the ignition source location may be seen in addition to the $T^*=1$ isotherm located in the reaction zone. Two $T^*=0.9$ isotherms, one resulting from the influence of the ignition source, and the other from the influence of the heat

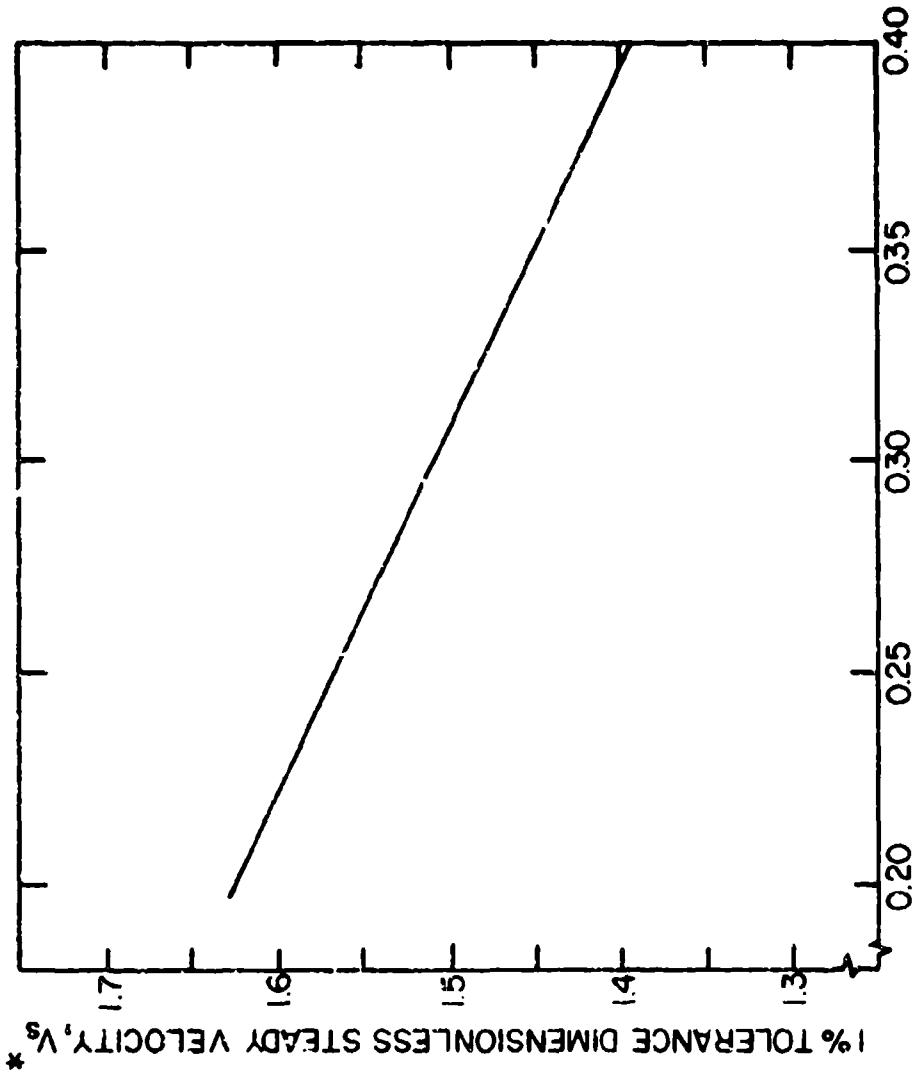

Figure 7 1% Tolerance Dimensionless Steady Reaction Propagation Velocity as a Function of PTFE-Lithium Mass Ratio

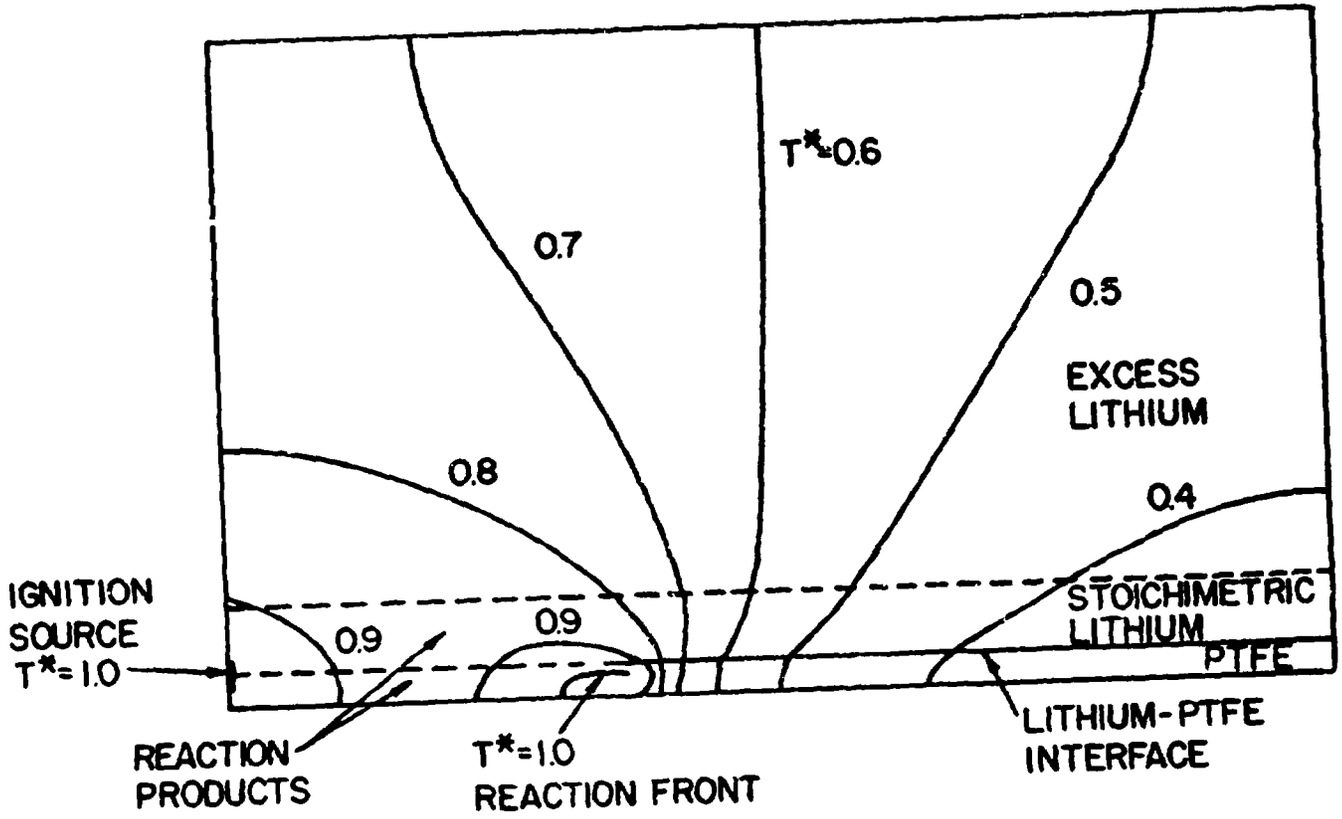

Figure 8 Dimensionless Temperature Profiles at 2.5% Tolerance Steady Conditions for L*/H* = 1.7 and PTFE-Lithium Mass Ratio = 0.206

generated within the reaztion zone, are also present. The temperature gradients within the PTFE are seen to be very much steeper than those within the lithium and reaction products. In addition, considerable heat conduction from the reaction products through the excess lithium to the PTFE in the region ahead of the reaction zone is evidenced.

For the numerical solutions of the dimensionless form of the two-dimensional model described above, the value of the unreacted PTFE mass fraction Z_T^*, at which the reaction was assumed to have gone to completion was taken as 0.1, corresponding to a product mass fraction of 0.9. Although this implies that only 90% of the original mass of PTFE present at each grid point in this layer was taken into account in the solutions, a decrease in this cutoff value to 0.05, corresponding to 95% of the PTFE mass reacted, had the effect of increasing the predicted 1% tolerance steady value of the dimensionless reaction propagation velocity by less than one percent. A PTFE mass fraction cutoff value of 0.1 was, therefore, used in these, as well as in subsequent, numerical solutions.

As previously indicated, the dimensionless form of the PTFE thermal decomposition rate law, Equation (2.17), was solved through the use of Euler's method [41]. Since this is a somewhat crude numerical representation of the solution of an ordinary differential equation, the method of Runge and Kutta [41] was also tried for comparison. Although the Runge-Kutta method is considerably more sophisticated, involving four additional calculations at each increment of the independent variable and a correspondingly longer total computation time, the resulting solution was seen to be

indistinguishable, to five significant figures, from that produced by Euler's method for independent variable increment sizes of interest. Since it was desired that computation time be minimized, Euler's method was, therefore, used in the numerical solution of the dimensionless form of the two-dimensional model.

CHAPTER III

EXPERIMENTAL INVESTIGATIONS

3.1 Experimental Apparatus

The test apparatus which contained the lithium-PTFE reaction sample is shown in Figure 9. This device was similar in most respects to the improved test apparatus used in the preliminary experiments previously described. The major component of the test apparatus was the sample tube, consisting of a 216 mm long, 28.6 mm outside diameter 304 stainless steel tube having 0.89 mm thick walls. The igniter plate, which was furnished with a tapped hole to accommodate the igniter, was fusion welded into one end of the sample tube. This component was constructed of 304 stainless steel as were the remaining elements of the test apparatus. The cap incorporated redundant high temperature Viton O-rings to form a seal at the end of the sample tube opposite the igniter plate. The 1 6 mm thick wafer was placed in the end of the sample tube adjacent to the cap in order to inhibit the flow of hot lithium and reaction products into the cap and associated plumbing after the reaction had taken place. A small quantity of lithium fluoride was also placed next to the wafer at the end of the PTFE sample in order to assist in this effort. The wafer was provided with several 1.6 mm diameter through-holes to allow pressure communication with the interior of the sample tube. The retainer, located at the igniter end of the sample tube, was so constructed as to allow access to the igniter (Holex Model 6102) while the retainer was in place. Four tie rods,

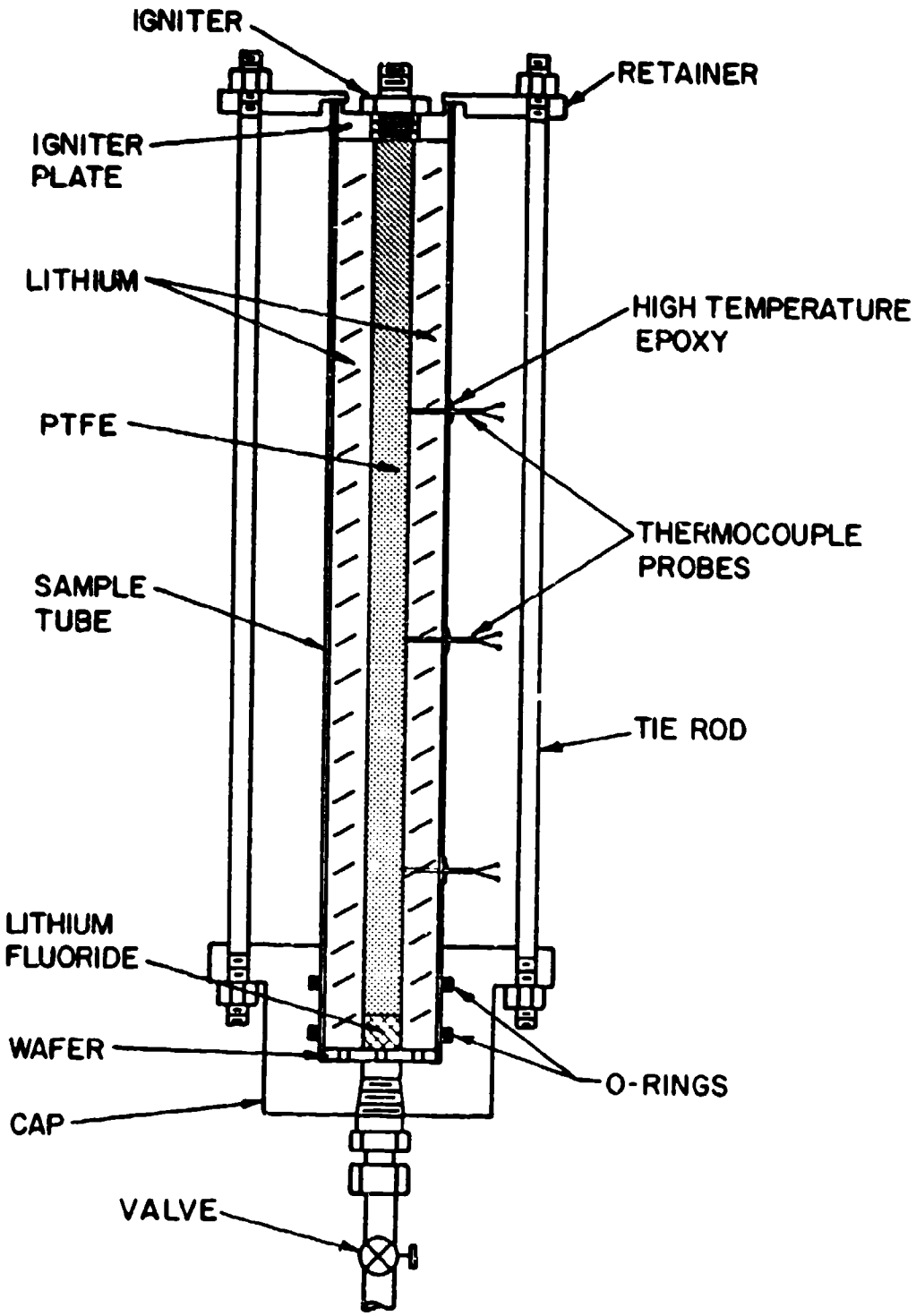

Figure 9 Sketch of Test Apparatus

two of which are shown in Figure 9, were used in conjunction with the retainer to hold the cap in place over the end of the sample tube. The chromel-alumel thermocouple probes, having 1.0 mm diameter sheaths, 0.15 mm diameter thermocouple wire, and exposed measuring junctions, were constructed from "Omegaclad" metal sheathed thermocouple wire. The probes were installed through the wall of the sample tube at 51 mm intervals, the thermocouple measuring junctions being located at the lithium-PTFE interface. The thermocouple probes were held in place by high temperature epoxy furnished by Omega Engineering, Incorporated.

In order to preclude problems should a high temperature lithium leak develop, the test apparatus was enclosed in a safety vessel while testing was in progress. The apparatus was mounted to the removable lid of the safety vessel, which was provided with feed-throughs for electric power and instrumentation signals along with tube fittings to allow communication with the sample tube and the interior of the safety vessel. A photograph of the test apparatus attached to the lid of the safety vessel is shown in Figure 10. The thermocouple leads are seen to have been connected to extension wires which terminate at a thermocouple jack panel also mounted to the safety vessel lid. The igniter power lead connected to the igniter at the top of the test apparatus is also visible in Figure 10.

A sketch of the overall test facility is shown in Figure 11. A solenoid valve was included in the test apparatus plumbing in order to allow isolation of the reaction sample prior to the initiation of each test run. Through the use of the argon tank, the vacuum pump, and the 3-way valves and associated plumbing, it was

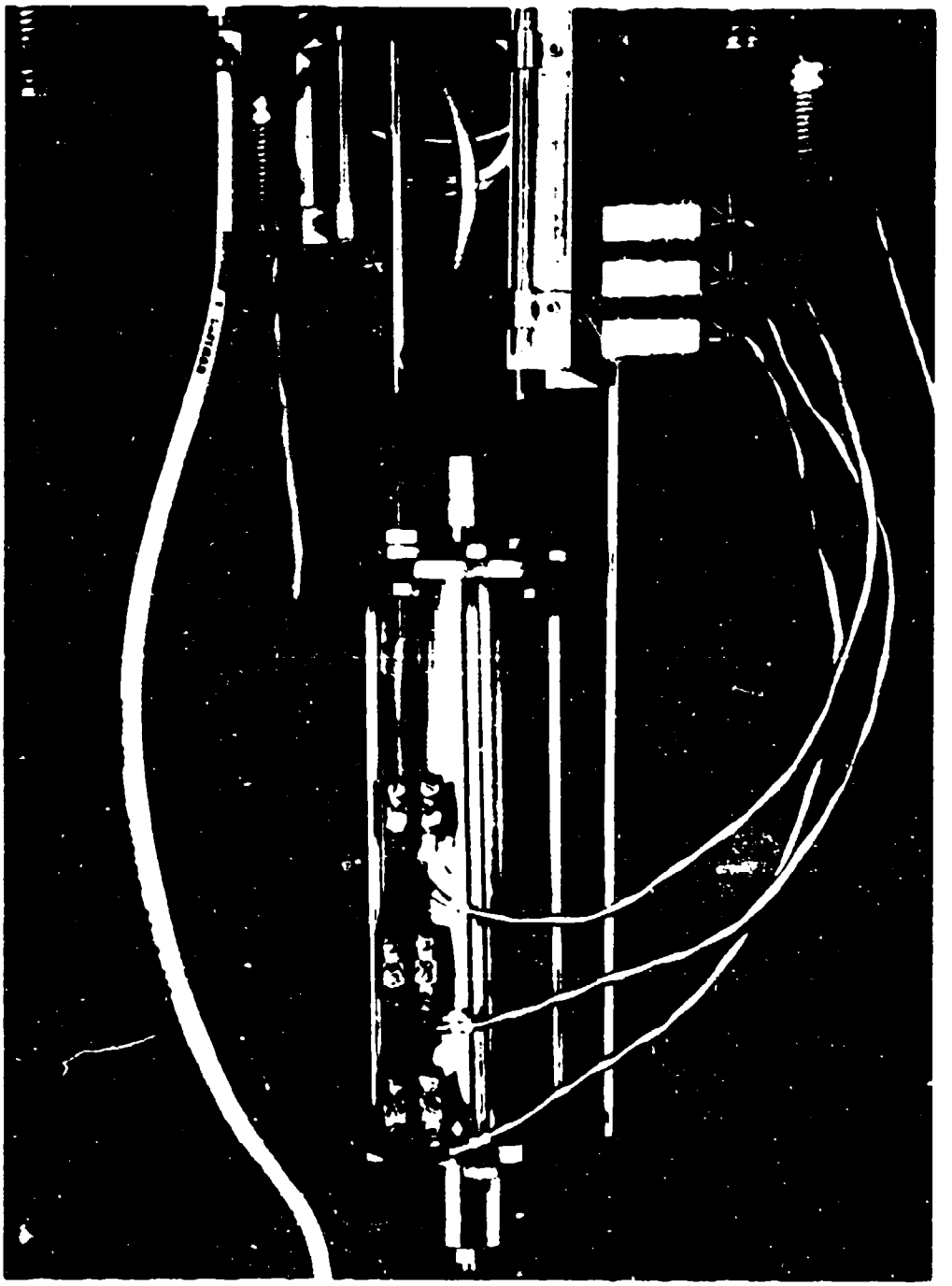

Figure 10 Photograph of Test Apparatus

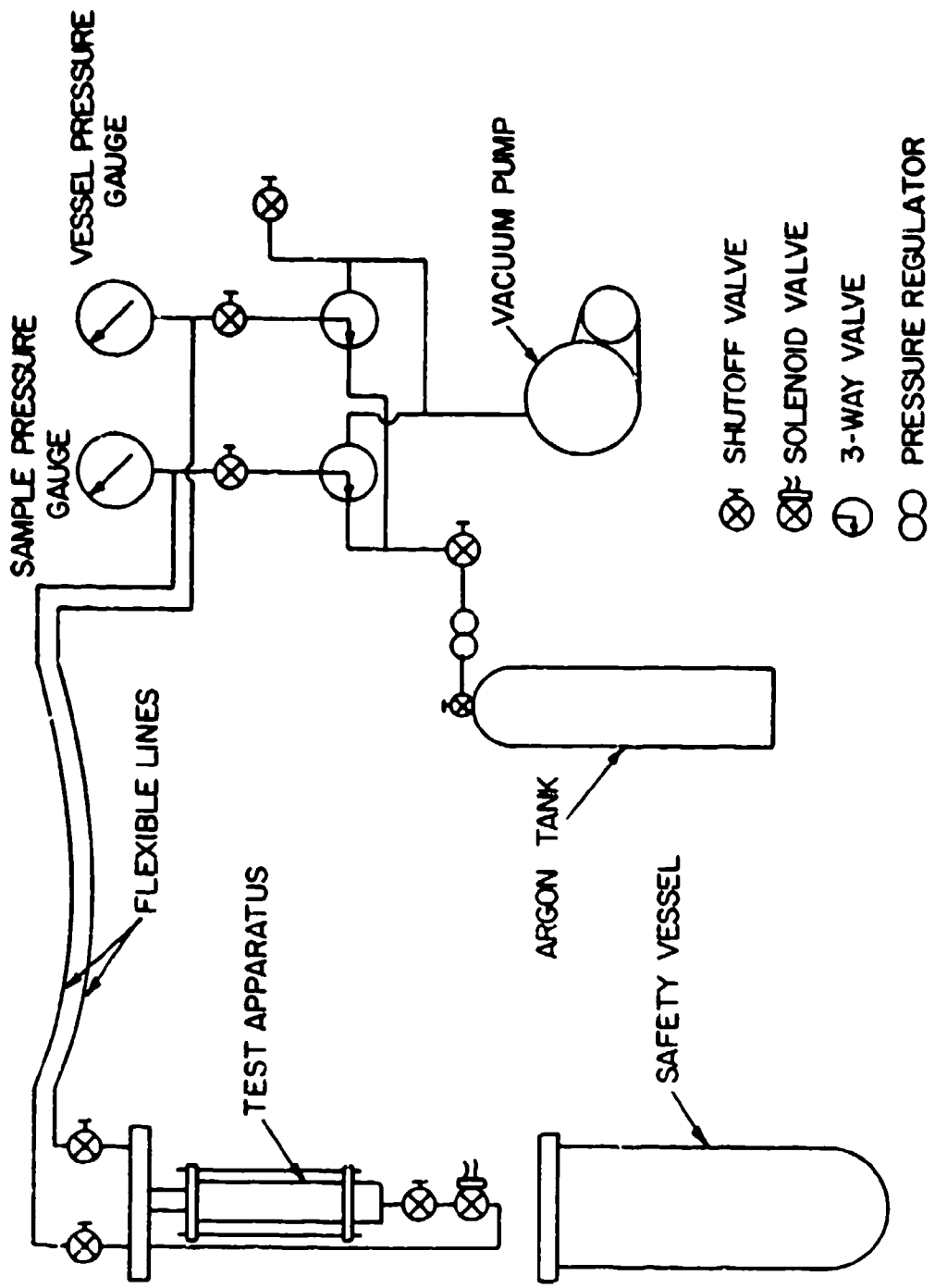

Figure 11 Sketch of Test Facility

possible to evacuate or pressurize the reaction sample and the interior of the safety vessel as desired, pressure gauges being provided to monitor the pressure levels present at these locations.

A photograph of the test facility is shown in Figure 12. The safety vessel and its lid with the test apparatus attached are visible at the left of this photograph. The control panel, on which were mounted the pressure gauges and associated plumbing, and the electric circuitry which controlled the operation of the solenoid valve and the igniter, may also be seen at the right of the photograph. Time-referenced records of the temperature levels present at the measuring junctions of the thermocouple probes during test runs were produced by recording the thermocouple analog voltage output signals on a Tektronix Model 564 dual trace storage oscilloscope and on a CEC Model 5-124 recording oscillograph. The voltage signals from all three thermocouples located at the lithium-PTFE interface in the reaction sample were recorded by the oscillograph, while only the thermocouple nearest the igniter and the thermocouple nearest the cap were connected to the oscilloscope; the oscillograph and the oscilloscope are visible on the table in the center of Figure 12. For some of the test runs, the digital timer located immediately below the control panel, as shown in Figure 12, was used in conjunction with the oscillograph and the oscilloscope to determine the reaction propagation velocity. This device was so designed as to utilize the thermocouple analog output voltage signals to start and stop a series of digital counters which measured and displayed the time elapsed between the arrival of the reaction front at subsequent thermocouple locations. Electrical noise problems, however, rendered

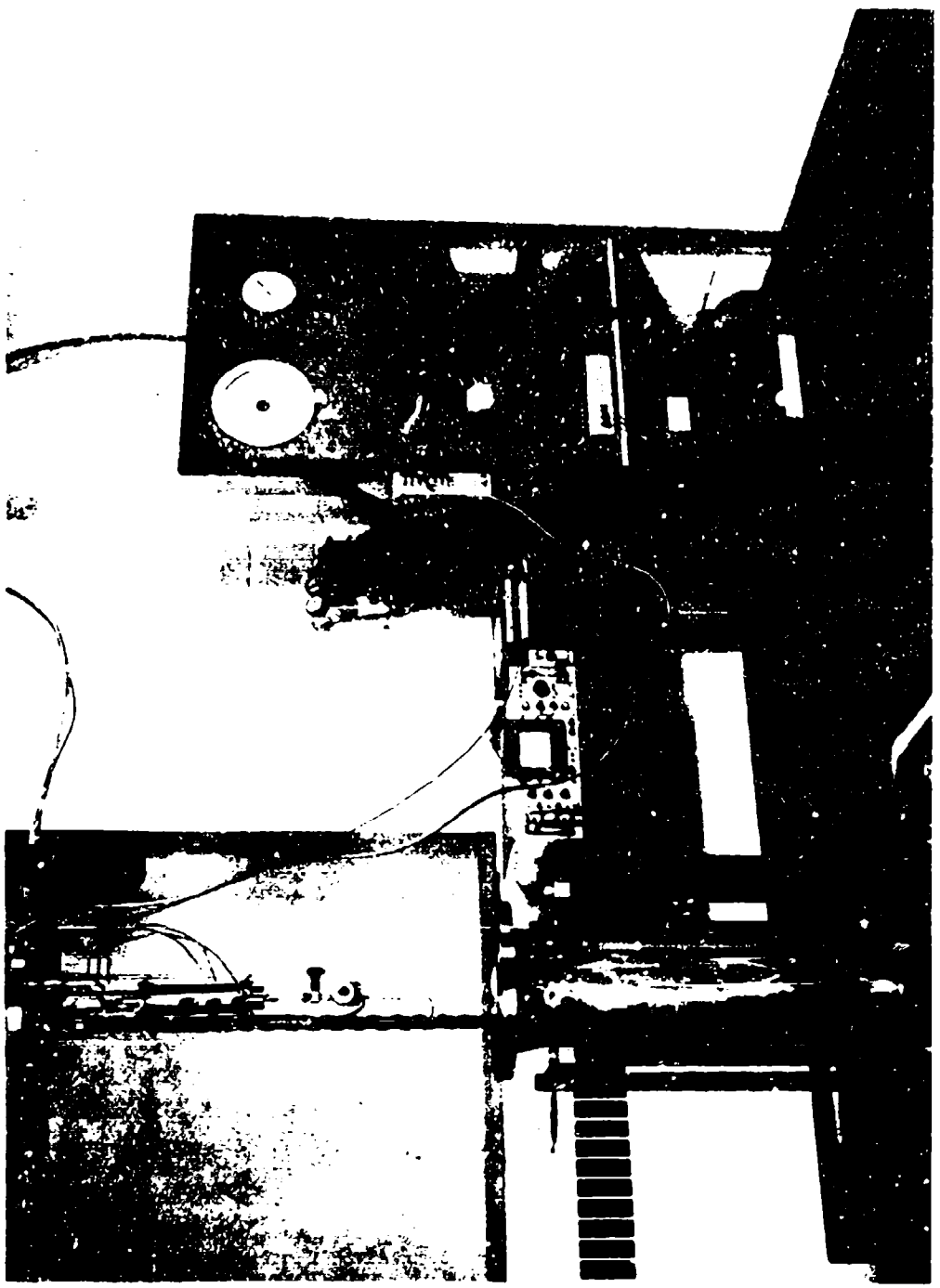

Figure 12 Photograph of Test Facility

the operation of the digital timer highly unreliable, and the use of this device was limited to the occasional corroboration of the records produced by the oscillograph and the oscilloscope. The vacuum pump located below the digital timer, and the argon tank positioned behind the control panel are also visible in Figure 12. The igniter was energized by a 12 volt output, series-parallel arrangement of four, 6-volt "Hot Shot" batteries also located behind the control panel.

In some of the test runs, it was attempted to measure and record the pressure occurring within the sample tube while the reaction was taking place. In order to accomplish this, two of the 304 stainless steel tie rods in the test apparatus were replaced by aluminum tie rods incorporating reduced cross-sectional area sections which were strain gauged. The two remaining stainless steel tie rods were allowed to remain in place but were installed loosely, acting as overpressure protection only. The strain gauges on the two aluminum tie rods were wired in series in order to minimize any unsymmetrical effects, and were included as one arm of a standard Wheatstone bridge. The bridge circuit was powered by a 6 volt dry cell battery and its output was suitably amplified and recorded on the CEC oscillograph. The system was calibrated prior to each test run by applying known pressures to the interior of an empty sample tube and observing the resulting output traces on the oscillograph record.

3.2 Experimental Procedure

The preparation for, and the conduction of a typical test run took place in the following manner: An empty sample tube, three thermocouple probes, and a core rod are shown in the photograph in Figure 13. The core rod, having been given a light coating of mineral oil to prevent lithium from adhering to its surface, was first installed in the empty sample tube by screwing the nut at the end of the rod into the igniter hole in the igniter plate. The core rod was thus positioned along the center of the sample tube. The thermocouple probes were then inserted through the holes in the wall of the sample tube until their measuring junctions contacted the surface of the core rod, and were secured in this position with high temperature epoxy. This sample tube-thermocouple probe-core rod assembly was then placed in an inert-atmosphere glove box (Vacuum Atmospheres Model HE-133-5) along with the cap and shutoff valve, the retainer, and the tie rods. Under an atmosphere of dry argon, liquid lithium at approximately 480 K was then poured into the empty sample tube, surrounding the core rod and the thermocouple probes. After the lithium had solidified and returned to room temperature, the core rod was removed and a dummy igniter installed in the igniter plate. The PTFE sample was then installed, followed by the small quantity of lithium fluoride. The wafer having been positioned in the end of the sample tube, the cap, the retainer, and the tie rods were put in place. The shutoff valve was then closed, and the test apparatus was removed from the glove box.

The test apparatus was then secured to the lid of the safety vessel, the thermocouple leads were connected to the thermocouple

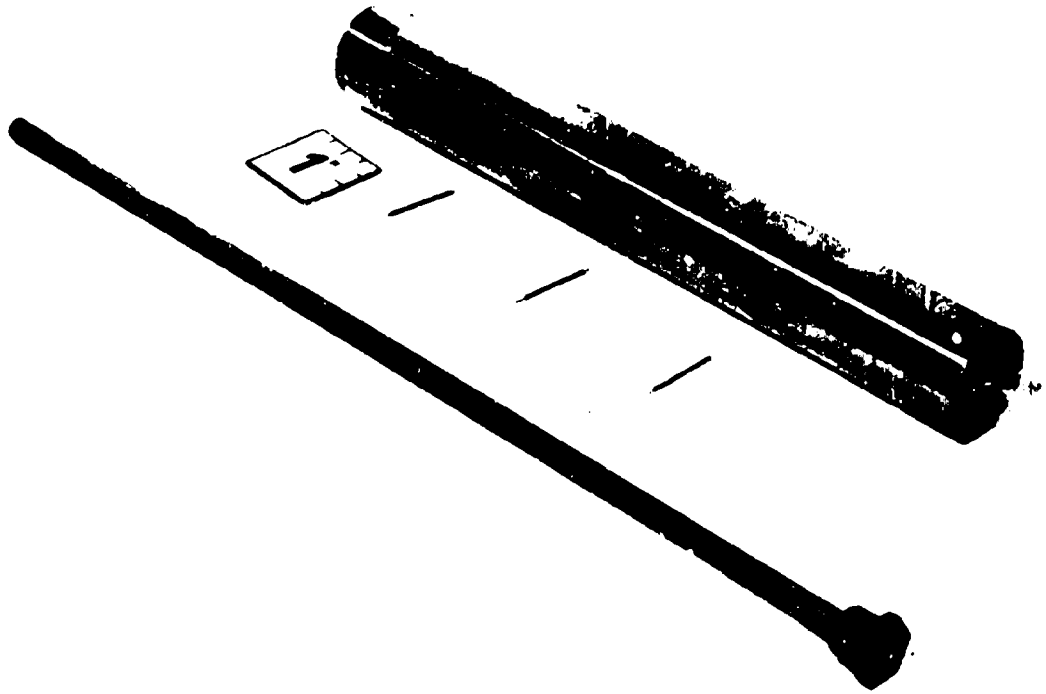

Figure 13 Photograph of Sample Tube, Thermocouple Probes, and Core Rod

jack panel through the extension wires, and the solenoid valve and attendant plumbing were installed. The dummy igniter was replaced by a live igniter, the igniter power lead was connected, and the shutoff valve was opened. The test apparatus was then lowered into the safety vessel by means of an electric hoist, and the lid of the vessel was secured.

The solenoid valve was then opened and the sample tube and the interior of the safety vessel were evacuated. After the attainment of the desired pressure level within the sample tube and the safety vessel, the solenoid valve was closed, as were the shutoff valves on the lid of the vessel and those adjacent to the pressure gauges on the control panel. The oscillograph chart drive was then started and the igniter was fired, electric power to the igniter being also utilized to trigger the oscilloscope sweep.

A sketch of the temperature-time record produced by the oscillograph for a typical test run is shown in Figure 14. As seen in this sketch, the arrival of the reaction front at each thermocouple location was attended by a rapid temperature rise, the reaction front reaching the location of the thermocouple nearest the igniter approximately 10 ms after electric power was applied to the igniter. From timing traces present on the oscillograph record, the time intervals between the arrival of the reaction front at each of the thermocouple locations were ascertained, and the reaction propagation velocity was determined by dividing the distance between the thermocouple measuring junctions by the time required for the reaction front to travel from one thermocouple location to the next. The total time required for the reaction front to travel from the

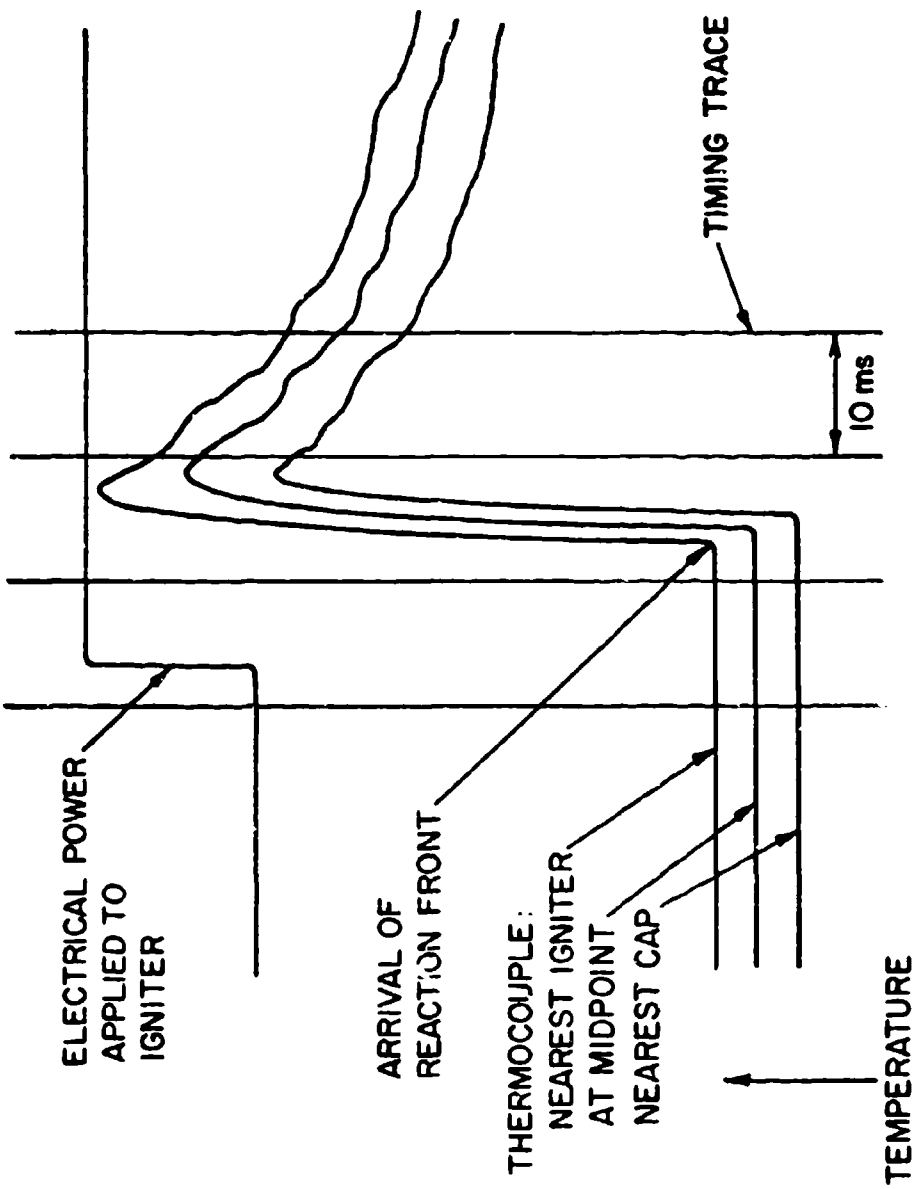

Figure 14 Sketch of Temperature-Time Record for a Typical Test Run

thermocouple nearest the igniter to the thermocouple nearest the cap was determined in a similar manner from the screen of the storage oscilloscope.

When the excess lithium and the reaction products contained in the sample tube had cooled to a reasonable temperature, the sample tube and the safety vessel were backfilled to atmospheric pressure with argon gas. The lid of the safety vessel and the attached test apparatus were then removed from the vessel. Finally, the test apparatus was disassembled, the sample tube and its contents being discarded, and the cap, the shutoff valve, and the associated plumbing being cleaned of residual lithium by water immersion in preparation for a future test run.

It should be pointed out, with reference to Figure 14, that the accuracy with which the reaction propagation velocity could be measured was seriously compromised by the nature of the temperature-time record. In order that the time intervals between the arrival of the reaction front at subsequent thermocouple locations could be determined, it was necessary to measure very small physical distances between the rapid temperature rises displayed on the record, which introduced an estimated $\pm 15\%$ uncertainty in the determination of the reaction propagation velocity. Since it was not possible to further increase the oscillograph chart speed, which would have allowed better resolution in these measurements, the development of the previously described digital timer was undertaken, it being theoretically possible to greatly increase the accuracy of the measurements through the use of this device. Although much effort was expended in attempts to rectify the situation, the digital timer

consistently malfunctioned under actual test conditions. For this reason, the temperature-time records produced by the oscillograph were used to determine the reaction propagation velocities in spite of the inherent inaccuracies present.

CHAPTER IV

EXPERIMENTAL AND THEORETICAL RESULTS

4.1 Experimental Conditions

In the experimental phase of this study, the effects of varying the diameter and density of the PTFE sample on the lithium-PTFE reaction propagation velocity were investigated. Density variation was accomplished by using solid PTFE rod for the highest density condition, and PTFE resin at several degrees of compaction for the less dense situations. The use of core rods of different sizes in the test preparation process allowed the diameter of the PTFE sample to be changed. Test runs were conducted with solid PTFE rod samples of 7.94 mm (5/16 inch), 6.35 mm (1/4 inch), 4.76 mm (3/16 inch), and 3.18 mm (1/8 inch) diameters, and with PTFE resin samples having diameters of 9.52 mm (3/8 inch), and 6.35 mm. Lithium metal obtained from the Lithium Corporation of America, with 99.8% minimum guaranteed purity, was used in all test runs.

The PTFE resin utilized in this investigation was Teflon Fluorocarbon resin manufactured by E. I duPont de Nemours and Company. Teflon 8A resin, having an average particle size of 0.52 mm, was used in the majority of the PTFE resin test runs. Teflon 8 resin, and Teflon 9B resin, with average particle sizes of 0.65 mm and 0.55 mm, respectively, were used in a small number of test runs in order to assess particle size effects. The largest portion of the Teflon 8A resin was obtained from duPont through normal commercial channels, while the remaining Teflon 8A resin, as well as the Teflon 8

and 9B resins, was furnished by the Technical Service Laboratory, Plastics Department, Fluorocarbons Division, at duPont. The apparent bulk density of these PTFE resins in their uncompacted form was of the order of 650 kg/m^3. As a result of the sample preparation process for the PTFE resin test runs, which involved lightly tamping the resin into the hole in the lithium sample left by the removal of the core rod, the density of the PTFE resin samples used in these test runs was increased to values in the range of 730-1200 kg/m^3. In order to preclude the possibility of a premature ignition caused by excessive lithium-PTFE contact pressure, no attempts were made to pack the PTFE resin to densities greater than 1200 kg/m^3.

In approximately 50% of the test runs involving solid PTFE rod, general purpose grade extruded PTFE rod obtained commerically from the Cadillac Plastic and Chemical Company was utilized. In the remainder of these test runs, extruded PTFE rod furnished by duPont's Technical Service Laboratory was used. The rod obtained from duPont consisted of samples fabricated from Teflon 8, 8A and 9B resins, these resins being from the same lots as were the resins furnished by duPont used in the PTFE resin test runs. The PTFE rod samples, as used in all but one of the test runs, were machine-turned to a diameter nominally 0.25 mm (0.010 inch) smaller than the core rod diameter in order to avoid interference with the lithium during installation.

In all but one case, the lithium-PTFE reaction test runs conducted in this investigation were carried out with the reaction sample under an initial vacuum. The ambient pressure level within

the sample tube immediately prior to the firing of the igniter in these test runs was approximately 10^{-3} bar.

4.2 Test Runs with 9.52 mm Diameter PTFE Samples

The test runs conducted with 9.52 mm (3/8 inch) diameter PTFE samples in all cases involved the use of PTFE resin. These test runs are summarized in Table 1. The first 5 runs listed in Table 1, Runs W-1 through W-5, are the preliminary tests described in Chapter I. For only these five runs, the reaction sample preparation process was not carried out in the inert-atmosphere glove box, but rather was done in the ambient atmosphere, the sample being continuously bathed in argon gas in order to minimize air contamination of the lithium. Further, no lithium fluoride was present in the reaction sample, and the wafer at the end of the sample tube was not utilized. Commercially obtained Teflon 8A resin at densities in the range 780-900 kg/m^3 was used in these test runs, yielding PTFE-lithium mass ratios from 0.226 to 0.261. The reaction propagation velocities listed in Table 1 for these five test runs, as well as for all other runs with 9.52 mm diameter PTFE samples, were determined by measuring the time required for the reaction front to travel from the thermocouple located nearest the igniter to the thermocouple nearest the cap. For all runs with 9.52 mm diameter PTFE samples, the reaction propagation velocities measured over the portion of the sample between the thermocouple nearest the igniter and the thermocouple at the midpoint of the sample, and between this thermocouple and the thermocouple nearest the cap were not significantly different from the reaction propagation velocity determined by using only the

Table 1

Summary of Lithium-PTFE Test Runs with 9.52 mm Diameter PTFE Resin Samples

Run Number	Lithium Mass (g)	PTFE Mass (g)	LiF Mass (g)	Resin Type	Resin Density (kg/m^3)	m_{PTFE}/m_{Li}	Propagation Velocity (m/s)	Comments
W-1	48.4	11.9	--	8A	820	0.246	30	Preliminary test, dirty sample
W-2	49.9	13.0	--	8A	900	0.261	45	Preliminary test, dirty sample
W-3	49.9	11.3	--	8A	780	0.226	--	Preliminary test, dirty sample propagation incomplete
W-4	48.6	11.8	--	8A	810	0.243	29	Preliminary test, dirty sample
W-5	50.0	11.5	--	8A	790	0.230	40	Preliminary test, dirty sample
M-1	50.7	11.0	1.2	8A	870	0.248	--	Timer malfunctioned, no data
M-2	49.5	10.5	4.1	8A	830	0.242	--	Timer malfunctioned, no data
M-3	44.9	11.6	2.2	8A	910	0.295	--	Timer malfunctioned, no data
M-4	51.3	11.5	1.7	8A	910	0.256	--	Timer malfunctioned, no data
M-5	51.0	12.7	1.8	8A	1000	0.285	--	Timer malfunctioned, no data
C-1	51.2	12.7	1.2	8A	1000	0.283	--	TC junctions 1.6 mm from int., propagation incomplete

Table 1 (Continued)

Run Number	Lithium Mass (g)	PTFE Mass (g)	LiF Mass (g)	Resin Type	Resin Density (kg/m^3)	m_{PTFE}/m_{Li}	Propagation Velocity (m/s)	Comments
C-2	51.3	12.5	1.9	8A	990	0.278	59	TC junctions 1.6 mm from int.
C-3	52.0	13.4	1.1	8A	1060	0.294	--	TC junctions 1.6 mm from int., nonsequential heating
C-4	52.0	13.7	1.1	8A	1080	0.301	--	TC junctions 1.6 mm from int., atmosphere: argon at 1 bar, nonsequential heating
C-5	52.2	13.3	1.1	8A	1050	0.291	--	TC junctions 1.6 mm from int., no propagation
C-6	52.3	13.1	1.3	8A	1030	0.286	37	
C-7	52.4	13.1	1.3	8A	1030	0.285	36	
C-8	52.0	13.2	1.5	8A	1040	0.290	32	10 s air exposure
C-9	52.6	13.1	1.2	8A	1030	0.285	55	60 s air exposure
C-10	52.4	14.1	1.3	8A*	1130	0.312	51	Maximum pressure = 12.4 bar
C-11	52.3	16.3	0.9	8*	1200	0.332	--	No propagation

*PTFE resin obtained from: Technical Service Laboratory, Plastics Department, Fluorocarbons Division, E. I. duPont de Nemours and Company

thermocouple nearest the igniter and the thermocouple nearest the cap. Under these relatively constant velocity conditions, the reaction propagation velocity measurements made using the two thermocouples nearest the ends of the reaction sample were considered more reliable due to the smaller effect of errors in the axial placement of the thermocouples. In these five test runs, the reaction propagation velocities were determined through the use of the CEC Oscillograph alone. As seen from Table 1, four of these five preliminary test runs were successful. In these runs, the reaction front propagated over the entire length of the reaction sample, allowing the reaction propagation velocity to be determined. During Run W-3, however, the reaction front propagated through only a portion of the sample before propagation ceased. This phenomenon was attributed to nonuniform packing of the PTFE resin, as previously described

In the next five test runs with the 9.52 mm diameter PTFE resin sample, Runs M-1 through M-5 in Table 1, it was attempted to measure the reaction propagation velocity by means of the digital timer alone. For these runs, commercially obtained Teflon 8A resin was used at densities from 830 to 1000 kg/m^3. The PTFE-lithium mass ratios present in these runs, as well as in all other runs in which lithium fluoride was used to inhibit the flow of high temperature lithium into the cap and associated plumbing, were computed by neglecting that portion of the lithium sample which surrounded the lithium fluoride. The PTFE-lithium mass ratios for runs M-1 through M-5 were thus 0.242 to 0.295. In each of these test runs, the digital timer malfunctioned, and no reaction propagation velocity data was obtained. In all subsequent test runs listed in

Table 1, as well as all test runs with PTFE sample diameters other than 9.52 mm, the CEC Oscillograph was used as the primary means of measuring the reaction propagation velocity, with the storage oscilloscope being utilized for corroboration of the results.

In an effort to make the results of the test runs less sensitive to suspected minor variations in the surface finish of the lithium at the lithium-PTFE interface, for Runs C-1 through C-5 the thermocouple measuring junctions were moved 1.6 mm (1/16 inch) away from the lithium-PTFE interface, into the lithium sample. Commercially obtained Teflon 8A resin at densities between 990 and 1080 kg/m^3 was used in these five runs, the resulting PTFE-lithium mass ratios being 0.278 to 0.301. In three of these test runs, C-2, C-3 and C-4 as shown in Table 1, the reaction front propagated over the entire length of the reaction sample. During Run C-1 the propagation of the reaction ceased before the end of the sample had been reached, and during Run C-5, the reaction was not initiated by the firing of the igniter. Of the three test runs in which the propagation was complete, only Run C-2 yielded reaction propagation velocity data. The analog records from the oscillograph for the remaining two test runs indicated that the reaction front arrived at the thermocouple located nearest the cap before arriving at the thermocouple located nearest the igniter. The atmosphere present within the sample tube immediately prior to the firing of the igniter in Run C-4 was argon at 1 bar pressure, as compared to the 10^{-3} bar vacuum present in all other runs. The nonsequential heating of the thermocouples was, however, not effected by this change in initial test conditions. It being physically impossible for the

reaction front to arrive at the thermocouple farthest from the igniter before arriving at the thermocouple nearest the igniter, assuming the thermocouples were located at the same radial position, the results of these test runs indicated that the reaction front is very thin in the radial direction, and that small errors in the positioning of the thermocouple measuring junctions at some distance from the lithium-PTFE interface are very critical. For this reason, the reaction propagation velocity measurement from Run C-2 was judged not reliable, and the thermocouple measuring junctions were located at the lithium-PTFE interface for all remaining test runs summarized in Table 1, as well as for all test runs with PTFE sample diameters other than 9.52 mm.

Test Runs C-6 and C-7 were conducted with commercially obtained Teflon 8A resin at 1030 kg/m^3 density, and PTFE-lithium mass ratios of 0.286 and 0.285, respectively. As seen from Table 1, the quantities of lithium, PTFE, and lithium fluoride used in these two runs were virtually identical. The reaction propagation velocity measured in Run C-6 was 37 m/s, and that in Run C-7, 36 m/s. From these results, it is indicated that under similar experimental conditions, the reaction propagation measurements are quite repeatable.

In the next two test runs shown in Table 1, an attempt was made to assess the effect of air contamination of the lithium sample on the reaction propagation velocity. These tests, Runs C-8 and C-9, resembled Runs C-6 and C-7 in that commercially obtained Teflon 8A resin was again used, and the amounts of lithium, PTFE, and lithium fluoride, the PTFE resin densities, and the PTFE-lithium mass ratios were similar. After the core rod had been withdrawn, but before the

installation of the PTFE resin during the preparation for Run C-8, the lithium sample in the sample tube was, however, removed from the inert-atmosphere glove box and exposed to the ambient air for a period of 10 seconds. The sample tube was then replaced in the glove box and the sample preparation process was continued in the normal manner. The reaction propagation velocity measured in this test run was 32 m/s. The preparation for Run C-9 was carried out in a like fashion, the lithium sample in this case being exposed to the ambient air for a period of 60 seconds, and the reaction propagation velocity being 55 m/s. The reaction propagation velocity in Run C-8, 32 m/s, compares favorably with that observed in the previous two similar test runs, while the reaction propagation velocity in Run C-9 was considerably higher. It is therefore indicated that the contamination of the lithium surface caused by prolonged air exposure has a noticeable effect on the reaction propagation velocity. The exact mechanism through which the reaction propagation process is altered in this situation is open to speculation. It, however, seems likely that the presence of the layer of lithium hydroxide formed on the surface of the lithium as a result of its exposure to moist ambient air [3] might well cause a significant change in the thermal conductivity of the lithium at the lithium-PTFE interface, and that this difference in thermal conductivity might be reflected by a change in the reaction propagation velocity.

Test Run C-10 was conducted in order that the effect of the use of Teflon 8A resin obtained from a different source might be assessed. The resin utilized in this run was furnished by the Technical Service Laboratory at duPont, and was capable of being

easily tamped to higher density than was the Teflon 8A resin obtained from duPont commercially. As shown in Table 1, the resin density was 1130 kg/m^3, the PTFE-lithium mass ratio was 0.312, and the reaction propagation velocity was 51 m/s for this test run. Since the resin density and the PTFE-lithium mass ratio for Run C-10 were approximately 10% higher than in Runs C-6 and C-7, made with commercially obtained Teflon 8A resin, it is impossible to ascertain whether the increase in the reaction propagation velocity was due to the change in test conditions alone, or to some difference in the PTFE resin itself.

In Run C-10, the pressure level present within the sample tube while the reaction was taking place was measured by means of the strain-gauged aluminum tie rods described in Chapter III. The maximum pressure level was 12.4 bar (180 psia). This pressure maximum occurred at approximately the same time that the reaction front reached the measuring junction of the thermocouple located nearest the igniter, indicating that the pressure wave propagated through the reaction sample more rapidly than did the reaction front. The pressure within the sample tube decreased approximately 10% from the maximum during the time required for the reaction front to travel from the thermocouple located nearest the igniter to the thermocouple located nearest the cap.

The final test run with the 9.52 mm diameter PTFE sample, Run C-11, was carried out in order to evaluate the effect of the use of a different type PTFE resin on the reaction propagation velocity. As shown in Table 1, Teflon 7 resin obtained from duPont's Technical

Service Laboratory was utilized in this run, the resin density and the PTFE-lithium mass ratio being again higher than in previous test runs. In Run C-11, the reaction was not initiated by the firing of the igniter. Whether this phenomenon was caused by a faulty igniter, or some property of the Teflon 8 resin is unknown.

Of the total of 21 test runs conducted with the the 9.52 mm diameter PTFE resin sample and summarized in Table 1, then, reaction propagation velocity data was obtained in 10 runs, and 9 of these 10 produced data judged reliable. The successful test runs in which commercially obtained Teflon 8A resin was utilized included 4 preliminary test runs, 2 air exposure runs, and 2 "baseline" runs with nearly identical experimental conditions. In these baseline runs, Runs C-6 and C-7, the average measured reaction propagation velocity was 36.5 m/s at an average PTFE-lithium mass ratio of 0.2855. The results of the short duration air exposure run (Run C-8) are in reasonable agreement with those of the baseline runs, while the results of the longer duration air exposure run (Run C-9) are not. The preliminary test runs were conducted at an average PTFE-lithium mass ratio of 0.245, and yielded an average measured reaction propagation velocity of 36 m/s. Although the actual exposure of the lithium to the ambient air during the preparation for these preliminary runs was probably of short duration, the results of these runs and their agreement with those of the baseline runs, are nevertheless of questionable reliability.

The reaction propagation velocity in the test run in which Teflon 8A resin obtained from the Technical Service Laboratory at duPont was used (Run C-10) was approximately 40% higher than that

observed in the baseline runs; the exact cause of this increase is not known. In this run, pressure measurements indicated that, at least in this particular situation, the velocity with which the pressure wave moves through the sample exceeds that with which the reaction front moves. The reaction was unable to be initiated by normal means in the one run conducted with Teflon 8 resin, although no obvious explanation for this phenomenon exists.

4.3 Test Runs with 6.35 mm Diameter PTFE Samples

In the test runs conducted with 6.35 mm (1/4 inch) diameter PTFE samples, PTFE in the form of resin, as well as in the form of solid rod was utilized. These test runs are summarized in Table 2 and Table 3, respectively. The reaction sample preparation process for all runs with 6.35 mm diameter PTFE samples was carried out in the inert-atmosphere glove box, and the analog output records from the CEC Oscillograph were used as the primary means of determining the reaction propagation velocity, data from the storage oscilloscope being used for corroboration. As was the case in the test runs with the 9.52 mm diameter PTFE samples, the reaction propagation velocity in all runs with 6.35 mm diameter PTFE samples was computed by using data obtained from the two thermocouples nearest the ends of the reaction sample, it being again observed that the reaction propagation velocity was reasonably constant over the entire instrumented length of these samples. The thermocouple measuring junctions for these runs were located at the lithium-PTFE interface, the PTFE-lithium mass ratios were computed by neglecting the lithium surrounding the lithium fluoride adjacent to the cap, and the pressure levels within

Table 2

Summary of Lithium-PTFE Test Runs with 6.35 mm Diameter PTFE Resin Samples

Run Number	Lithium Mass (g)	PTFE Mass (g)	LiF Mass (g)	Resin Type	Resin Density (kg/m^3)	$\frac{m_{PTFE}}{m_{Li}}$	Propagation Velocity (m/s)	Comments
D-1	56.6	6.1	0.6	8A	1060	0.121	42	
D-2	56.5	6.0	0.9	8A	1050	0.119	62	
D-3	56.2	4.8	0.3	8A*	730	0.083	---	Nonsequential heating
D-4	56.2	5.0	0.9	8A*	830	0.096	--	Nonsequential heating
D-5	56.1	5.7	0.6	8A	1010	0.116	--	Contaminated lithium, no propagation
D-6	56.5	6.1	0.6	8A	1080	0.123	49	Maximum pressure = 15.9 bar

*PTFE resin obtained from: Technical Service Laboratory, Plastics Department, Fluorocarbons Division, E. I. duPont de Nemours and Company

Table 3

Summary of Lithium-PTFE Test Runs with 6.35 mm Diameter PTFE Rod Samples

Run Number	Lithium Mass (g)	PTFE Mass (g)	LiF Mass (g)	PTFE Source	m_{PTFE}/m_{Li}	Propagation Velocity (m/s)	Comments
E-1	56.6	9.3	0.9	Commercial	0.193	70	Large gap at interface
E-2	57.0	11.6	0.9	Commercial	0.224	57	
E-3	55.0	12.2	0.8	Teflon 8A	0.229	42	Maximum pressure = 19.3 bar
E-4	56.0	12.2	0.4	Teflon 8A	0.225	--	Lithium leak during run, cutting oil used on PTFE
E-5	55.2	12.0	0.5	Teflon 8A	0.224	50	Circumferential TC locations
E-6	55.4	12.4	0.5	Teflon 8	0.231	--	Propagation incomplete, cutting oil used on PTFE
E-7	55.7	12.3	0.5	Teflon 9B	0.228	--	No propagation, cutting oil used on PTFE
E-8	56.4	11.6	0.5	Commercial	0.219	41	Lithium leak during run, maximum pressure = 29.0 bar
E-9	56.6	11.6	0.5	Teflon 8	0.218	--	Propagation incomplete, maximum pressure = 15.2 bar
E-10	56.5	11.8	0.6	Teflon 9B	0.219	49	

the sample tubes immediately prior to the firing of the igniter were approximately 10^{-3} bar.

As shown in Table 2, all test runs conducted with PTFE resin samples of 6.35 mm diameter involved the use of Teflon 8A resin. In the first two runs listed in Table 2, Runs D-1 and D-2, commercially obtained Teflon 8A resin was utilized at densities of 1060 and 1050 kg/m^3, respectively. The amounts of lithium, PTFE, and lithium fluoride present in these two runs were similar, as were the PTFE-lithium mass ratios. The reaction propagation velocity measured in Run D-1 was 42 m/s, and that in Run D-2, 62 m/s.

The next two test runs with the 6.35 mm diameter PTFE resin sample were carried out in order to investigate the effect of reduced PTFE resin density on the reaction propagation velocity. As shown in Table 2, test runs D-3 and D-4 involved equal amounts of lithium, and similar amounts of lithium fluoride. These runs were conducted with PTFE resin densities of 730 and 830 kg/m^3, and PTFE-lithium mass ratios of 0.083 and 0.096, respectively, Teflon 8A resin obtained from the Technical Service Laboratory at duPont being utilized. Since the thermocouple measuring junctions were heated nonsequentially in Runs D-3 and D-4, the thermocouple nearest the cap indicating a sharp temperature rise before the thermocouple nearest the igniter, no reaction propagation velocity data resulted. Post-test run inspection of the reaction sample showed that the PTFE resin had been blown toward the opposite end of the sample tube by the firing of the igniter. The exact resin density below which the reaction will not propagate normally is, no doubt, a function of the type of PTFE resin utilized. However, in these two test runs it was demonstrated that,

at sufficiently low PTFE resin densities, the configuration of the PTFE sample is altered by the action of the igniter to such an extent that normal reaction propagation is prohibited.

Test Runs D-5 and D-6 were the final two runs involving 6.35 mm diameter PTFE samples, as shown in Table 2. Commercially obtained Teflon 8A resin was used in these runs, and experimental conditions were made similar to those present in Runs D-1 and D-2 in an attempt to establish a more meaningful baseline for the PTFE resin test runs in this PTFE sample diameter. In Run D-5, the reaction was not initiated by the firing of the igniter. This phenomenon was attributed to the inadvertent exposure of the lithium sample to ambient air for a period of several hours during the sample preparation process. Test Run D-6, in which the PTFE resin density was 1080 kg/m^3, and the PTFE mass ratio was 0.123, yielded a measured reaction propagation velocity of 49 m/s. The pressure level within the sample tube during the reaction propagation process was also measured in this run, the maximum pressure present being 15.9 bar (230 psia). In Run D-6, no pressure was evidenced until after the reaction front had passed the measuring junction of the thermocouple located nearest the cap, indicating that, in this run, the reaction front propagated through the sample at least as rapidly as did the pressure wave.

From the results of the test runs conducted with 6.35 mm diameter PTFE resin samples, as shown in Table 2, it was observed that the reaction front will not propagate normally at sufficiently low PTFE resin densities. The three successful baseline runs (Runs D-1, D-2 and D-6), with an average PTFE-lithium mass ratio of 0.121,

yielded an average measured reaction propagation velocity of 51 m/s, and pressure measurements made during Run D-6 indicated that under the experimental conditions shown in Table 2, the reaction front moves through the reaction sample at a velocity not less than that of the pressure wave.

Shown in Table 3 is a summary of the test runs conducted with 6.35 mm diameter solid PTFE rod samples. For these runs, commercial PTFE rod obtained from the Cadillac Plastic and Chemical Company, as well as PTFE rods fabricated from Teflon 8, Teflon 8A, and Teflon 9B resins by the Technical Service Laboratory at duPont, were used in the construction of the PTFE samples. As in the test runs with PTFE resin samples of the same diameter, the pressure level within the sample tube at the time of the firing of the igniter in these runs was approximately 10^{-3} bar. The reaction samples were again prepared in the inert-atmosphere glove box, the thermocouple measuring junctions being placed at the lithium-PTFE interface. The reaction propagation velocities in these runs were determined from the analog output records from the CEC Oscillograph and were confirmed by the data from the storage oscilloscope, and the lithium surrounding the LiF at the end of the sample was neglected in the computation of the PTFE-lithium mass ratios.

Test Runs E-1, E-2, and E-8 were conducted with 6.35 mm diameter commercial solid PTFE rod samples, as shown in Table 3. For Run E-1, the PTFE sample was machined to a diameter 0.50 mm (0.020 inch) smaller than the core rod diameter in order to insure that no interference between the lithium and the PTFE samples during the installation of the PTFE would occur. A rather large gap between the

lithium and the PTFE at the lithium-PTFE interface was thus created. Although the reaction front propagated in a normal manner in this test run, at a measured reaction propagation velocity of 70 m/s, this result was judged unreliable due to the excessive clearance between the lithium and PTFE samples. The PTFE samples for all other test runs involving solid PTFE rod were machined to a diameter nominally 0.25 mm (0.010 inch) smaller than the core rod, which reduced the clearance between the samples while still preventing an interference fit. Test Runs E-2 and E-8 were conducted with PTFE-lithium mass ratios of 0.224 and 0.219, respectively. The measured reaction propagation velocity in Run E-2 was 57 m/s, and that in Run E-8, 41 m/s. From a leak which developed during Run E-8, a quantity of hot lithium was deposited in the vicinity of one of the strain-gauged aluminum tie rods. The thermocouple extension wires were uneffected, however, and the reaction propagation velocity measurement was judged reliable.

In Runs E-3, E-4 and E-5, the PTFE samples were constructed from solid rods fabricated from Teflon 8A resin by the Technical Service Laboratory at duPont. During Run E-4, a lithium leak onto the thermocouple extension wires prevented reaction propagation data from being obtained. As a result of this lithium leak, and the attendant destruction of the thermocouple extension wires, it was not possible to ascertain whether the propagation of the reaction front occurred normally. In addition, it was later determined that cutting oil had been used on the PTFE sample during final sizing, it being felt that the presence of a small quantity of residual oil on the PTFE sample might well effect the reaction propagation

process. In Runs E-3 and E-5, the reaction front propagated through the sample in a normal manner at measured propagation velocities of 42 m/s and 50 m/s, respectively, as shown in Table 3. For Run E-5, two additional thermocouples were placed at the same axial position as the thermocouple at the midpoint of the sample tube, but at different circumferential locations around the lithium-PTFE interface. The reaction front was observed to arrive at the measuring junctions of these three thermocouples simultaneously, indicating that the propagation of the reaction front is axisymmetric.

Solid PTFE rod fabricated from Teflon 8 resin at duPont's Technical Service Laboratory was used in the construction of the PTFE samples for Runs E-6 and E-9, as shown in Table 3. In both of these runs, the reaction front did not propagate over the entire length of the sample. In Run E-6, this may have been in part due to the fact that cutting oil was used during the final sizing of the PTFE sample; no explanation is offered in the case of Run E-9.

Test Runs E-7 and E-10 involved the use of solid PTFE rod fabricated from Teflon 9B resin by the Technical Service Laboratory at duPont. Cutting oil was used in the machining of the PTFE sample for Run E-7, and the reaction was not initiated by the firing of the igniter. Test Run E-10 was conducted successfully at a PTFE-lithium mass ratio of 0.219, the measured reaction propagation velocity being 49 m/s.

Reaction pressure measurements were made during Run E-3 with Teflon 8A rod, Run E-8 with commercial rod, and Run E-9 with Teflon 8 rod. Since the propagation of the reaction in Run E-9 was incomplete, no meaningful conclusions may be drawn from this

pressure measurement. In light of the fact that strain gauges are very temperature sensitive, it is felt that the presence of a hot lithium leak near one of the strain gauges during Run E-8 rendered this pressure measurement also meaningless. The maximum pressure measured during Run E-3 was 19.3 bar, the indication of this pressure occurring well after the reaction front had passed the location of the thermocouple nearest the cap. It was therefore concluded that, under the experimental conditions present in this run, as shown in Table 3, the pressure wave does not precede the reaction front through the sample.

From the results of the test runs conducted with 6.35 mm diameter solid PTFE rod samples, it is seen that in no case did the propagation of the reaction front occur normally in runs involving PTFE samples on which cutting oil had been used during machining. It is therefore concluded that the presence of small quantities of residual oil on the surface of the PTFE sample in some manner effects the reaction propagation process. Neglecting the results of Run E-1, in which the large clearance between the lithium and PTFE samples was present, the successful test runs with commercial PTFE rod were carried out at an average PTFE-lithium mass ratio of 0.222, and yielded an average measured reaction propagation velocity of 49 m/s. The average PTFE-lithium mass ratio for the successful test runs with PTFE rod samples fabricated from Teflon 8A resin was 0.226, and the average reaction propagation velocity was 46 m/s, while for the successful run conducted with the Teflon 9B rod sample, the PTFE-lithium mass ratio was 0.219 and the measured average reaction

propagation velocity was 49 m/s. Neither of the test runs conducted with Teflon 8 rod samples were successful.

It is believed that, within the limits of experimental error, the results of the runs with the commercial rod samples may not be distinguished from the results of the runs with the Teflon 8A rod samples, or those of the run with the Teflon 9B rod sample. For this reason, the experimental results for the test runs involving 6.35 mm diameter solid PTFE rod samples may be summarized by the average values from the successful runs, which are a PTFE-lithium mass ratio of 0.223, and a reaction propagation velocity if 47.8 m/s.

4.4 Test Runs with PTFE Samples of Other Diameters

In addition to the test runs involving 9.52 mm diameter, and 6.35 mm diameter PTFE samples, test runs were conducted with 3.18 mm (1/8 inch) diameter, 4.76 mm (3/16 inch) diameter, and 7.94 mm (5/16 inch) diameter PTFE samples. These runs, in which commercial PTFE rod was used, are summarized in Table 4. The measuring junctions of the thermocouples used in these test runs were located at the lithium-PTFE interface, the preparation of the samples was carried out in the inert-atmosphere glove box, and the PTFE samples were machined to a diameter nominally 0.25 mm (0.010 inch) smaller than the core rod diameter to avoid an interference fit. The lithium surrounding the LiF at the end of the sample was neglected in the computation of the PTFE-lithium mass ratios, and the pressure level within the sample tube at the time of the firing of the igniter in these runs was approximately 10^{-3} bar. The reaction propagation velocities were

Table 4

Summary of Lithium-PTFE Test Runs with Commercial PTFE Rod Samples

Run Number	PTFE Diameter (mm)	Lithium Mass (g)	PTFE Mass (g)	LiF Mass (g)	m_{PTFE}/m_{Li}	Propagation Velocity (m/s)	Comments
H-1	3.18	58.6	2.65	0.1	0.047	--	Reaction zone deceleration, maximum pressure = 3.8 bar
H-2	3.18	59.1	2.65	0.1	0.047	--	Reaction zone deceleration, no indicated pressure rise
J-1	4.76	58.0	6.6	0.1	0.117	25	
J-2	4.76	58.1	6.4	0.1	0.113	19	Maximum pressure = 14.8 bar
K-1	7.94	54.1	18.6	0.4	0.360	76	

determined from the analog output records from the CEC Oscillograph, data obtained from the storage oscilloscope being used for confirmation when possible.

As shown in Table 4, Runs H-1 and H-2 were conducted with 3.18 mm diameter PTFE rod samples under similar experimental conditions, the PTFE-lithium mass ratio for both runs being 0.047. In these runs, the reaction propagation velocity measured over that portion of the sample between the thermocouple nearest the igniter and the thermocouple at the midpoint of the sample was considerably higher than that measured over the portion between the thermocouple at the midpoint and the thermocouple nearest the cap. The reaction zone was thus observed to be declerating as it propagated through the sample, it being therefore concluded that normal reaction propagation is not possible at PTFE-lithium mass ratios of this magnitude. The pressure within the sample tube during these runs was also measured. A maximum pressure of 3.8 bar in Run H-1 occurred well after the reaction front had passed the location of the thermocouple nearest the cap, indicating that the pressure wave does not precede the reaction front through the sample in runs under these experimental conditions. Although the reaction front did propagate over the entire length of the sample in Run H-2, no pressure rise above the initial condition of approximately 10^{-3} bar was observed.

Test runs J-1 and J-2 were carried out with 4.76 mm diameter PTFE rod samples under similar experimental conditions, at PTFE-lithium mass ratios of 0.117 and 0.113, respectively. As shown in Table 4, the reaction propagation measured in Run J-1 was 25 m/s, and that in Run J-2, 19 m/s. One of the leadwires from the thermocouple nearest the

igniter was broken during the preparation for Run J-1, and a similar occurrence rendered the thermocouple nearest the cap inoperable in Run J-2. In these two test runs, the reaction propagation velocity was therefore determined using data obtained from the thermocouple located at the midpoint of the sample tube, and the one other functional thermocouple. The pressure within the sample tube was measured during Run J-2, the maximum pressure of 14.8 bar occurring after the reaction front had passed the location of the thermocouple nearest the cap. The pressure wave thus did not propagate through the sample at a more rapid velocity than did the reaction front in this run. Although the reaction front propagated over the entire length of the sample in these two test runs, the character of the propagation appeared weak, as indicated on the analog output record from the CEC Oscillograph by a rather slow rate of temperature rise caused by the arrival of the reaction front at the locations of the functional thermocouples. In light of this observation, it is concluded that the propagation of the reaction is marginal under the conditions of Runs J-1 and J-2, as shown in Table 4, and that the results of these two runs are of questionable reliability.

The PTFE rod sample utilized in Run K-1 was of 7.94 mm diameter, as shown in Table 4. At a PTFE-lithium mass ratio of 0.360, the measured reaction propagation velocity was 76 m/s, this result having been determined using the data from the two thermocouples located nearest the ends of the sample. Due to the rather high PTFE-lithium mass ratio, local melting of the sample tube, accompanied by sizeable lithium leaks, occurred during this run. The thermocouple

extension wires were, however, not damaged, and the reaction propagation velocity measurement was judged reliable.

4.5 Experimental-Theoretical Comparisons

In order to compare the predictions of the model with the experimental results, it is first necessary to numerically evaluate the characteristic time and the characteristic velocity, as used in Equation (2.27). The characteristic time, t_{ch}, is defined, as described in Chapter II, as the time required to thermally decompose 90% of an initial amount of PTFE at the stoichiometric adiabatic flame temperature at one atmosphere total pressure. The PTFE thermal decomposition rate law is given by the following relationship:

$$\frac{dZ_T^*}{dt} = - A_o Z_T^* e^{-E_a/RT} \tag{2.6}$$

For the situation in which the temperature is constant and equal to the stoichiometric adiabatic flame temperature at standard conditions, T_{af}, the product of the frequency factor and the exponential term in the above equation is also a constant, and is defined as:

$$K = A_o e^{-E_a/RT_{af}} \tag{4.1}$$

The substitution of Equation (4.1) into Equation (2.6) yields:

$$\frac{dZ_T^*}{dt} = - K Z_T^* \quad . \tag{4.2}$$

Rearranging and integrating the above equation, and applying the initial condition:

$$t = 0 \quad ; \quad Z_T^* = 1 \quad , \tag{4.3}$$

results in the following expression for the undecomposed PTFE mass fraction as a function of time:

$$\ell n\ Z_T^* = -\ Kt \quad . \tag{4.4}$$

Under the condition that the thermal decomposition of the PTFE is 90% complete, the value of Z_T^* is 0.10, and the corresponding time is the characteristic time, as given by:

$$t_{ch} = \frac{-\ \ell n(0.10)}{K} \quad . \tag{4.5}$$

From Reference [37]:

$$A_o = 3.0 \times 10^{19}\ s^{-1}$$

and

$$E_a = 3.475 \times 10^{5}\ J/mol \quad .$$

The stoichiometric adiabatic flame temperature under standard conditions is 1966 K, as previously described. These quantities may be combined to yield:

$$\frac{E_a}{RT_{af}} = 21.245 \quad , \tag{4.6}$$

and, from Equation (4.1):

$$K = 1.7805 \times 10^{-10}\ s^{-1} \quad . \tag{4.7}$$

The value of t_{ch} is then determined from Equation (4.5):

$$t_{ch} = 1.293 \times 10^{-10}\ s \quad . \tag{4.8}$$

It is now desired to evaluate the characteristic velocity as given by the following expression:

$$V_{ch} = \sqrt{\frac{\alpha_T}{t_{ch}}} \quad . \tag{2.27}$$

Using the value of the thermal diffusivity of PTFE as given in Reference [43], and the characteristic time as evaluated above, this expression is evaluated to yield:

$$V_{ch} = 29.4 \text{ m/s} \quad . \tag{4.9}$$

A summary of the results of the successful lithium-PTFE test runs is shown in Table 5. The values of the PTFE-lithium mass ratios and the measured reaction propagation velocities given in Table 5 are averages for all successful test runs with PTFE samples of the diameter and type listed with the exception of the data for the 7.94 mm diameter PTFE sample, with which only one successful test run was conducted. It may be noted from this table that, neglecting the data from the one test run with the 7.94 mm diameter PTFE rod sample, the measured reaction propagation velocities are seen to decrease with increasing PTFE-lithium mass ratio, a trend which was predicted by the model. The predicted dimensionless reaction propagation velocities shown in Table 5 were evaluated from the linear relationship for V_S^* as a function of PTFE-lithium mass ratio, Equation (2.28), and the dimensional reaction propagation velocities were determined through the following rearrangement of Equation (2.26):

$$V_S = V_S^* \, V_{ch} \quad . \tag{4.10}$$

Table 5

Summary of Results of Successful Lithium-PTFE Test Runs

PTFE Sample Diameter (mm)	PTFE Sample Type	Number of Successful Test Runs	Average PTFE-Li Mass Ratio	Average Measured Propagation Velocity (m/s)	Predicted Dimensionless Propagation Velocity, V_S^*	Predicted Propagation Velocity, V_S (m/s)	Error (%)
6.35	Resin	3	0.121	51.0	1.72	50.6	0.8
6.35	Rod	5	0.223	47.8	1.60	47.0	1.7
9.52	Resin	9	0.286	36.5	1.53	45.0	23.3
7.94	Rod	1	0.360	76.0	1.44	42.3	44.3

The error values given in Table 5 are the absolute value of the difference between the measured and predicted velocities divided by the measured velocity for each of the PTFE sample diameters and types listed.

In the numerical solution of the model, the properties of the PTFE were taken as those of the solid, as previously described. It was, therefore, felt that the experimental results from test runs in which solid PTFE rod samples were used should provide a more meaningful test of the model than the results of the runs in which PTFE resin samples were utilized. From Table 5 it is seen that for the test runs involving 6.35 mm diameter PTFE rod samples, the predicted reaction propagation velocity is 1.7% lower than the average experimentally measured value. In contrast to this close agreement is the result of the test run with the 7.94 mm diameter PTFE rod sample, which is a measured reaction propagation velocity approximately 44% higher than that predicted the model. No explanation for this large discrepancy is offered, although the fact that only one test run with this diameter PTFE rod sample was conducted casts some doubt on the reliability of the experimental results.

No attempt was made to adjust the model to account for situations in which PTFE resin samples were used since the estimation of the thermal diffusivity of a packed granular bed yields values which are approximate at best, and it was previously found that the results of the model are a strong function of the value used for the thermal diffusivity of the PTFE. The predicted reaction propagation velocities for the test runs with PTFE resin samples were arrived at through the use of the properties of solid PTFE in the model, and

were included in Table 5 for comparison purposes only. The accuracy with which the reaction propagation velocity was predicted for the test runs involving PTFE resin samples is, therefore, rather surprising, in light of the uncertainty in the value of α_T, as well as the fact that, for the 6.35 mm diameter PTFE resin test runs, the predicted value of V_S^* was obtained by extrapolating the linear relationship given by Equation (2.28) beyond the range of analytical investigation.

Under experimental conditions, the aspect ratio of the lithium-PTFE reaction samples, defined as the length of the sample divided by its radius, was approximately 15. From the results of the numerical solution of the model previously described, however, it was indicated that the predicted dimensionless steady reaction propagation velocity was not a function of aspect ratio for values of L^*/H^* of 10 and greater. It is, therefore, believed that this lack of geometric similarity is not a significant source of error. From Table 5 it may be seen that the reaction propagation velocity was predicted more accurately for the test runs with 6.35 mm diameter PTFE samples than for the runs involving PTFE samples of other diameters. A possible explanation is the fact that the model was cast in cartesian coordinates, the surface to volume ratio of the PTFE sample being therefore only a function of the thickness of the PTFE, which was held constant. The surface to volume ratio of the cylindrical PTFE samples used in the test runs, however, varies inversely with diameter. Additionally, it is estimated that an error in the axial positioning of the thermocouples of approximately $\pm$ 3 mm was possible during the preparation for the test runs. For the nominal 102 mm instrumented

length of the sample tube, this positioning error would be reflected as a ± 6% error in the reaction propagation velocity measurements. The estimated total error in these measurements, due to thermocouple positioning errors and the limitations of the instrumentation, was ± 15 percent.

The purpose of the pressure measurements made during several of the test runs was not to precisely determine the pressure level at which the reaction took place, as this was beyond the capability of the experimental apparatus. Rather, these measurements were undertaken in order to assess whether the reactants ahead of the reaction front are preheated by thermal conduction only, as postulated in the mechanism, or by the presence of a hot gas pressure wave which precedes the reaction front through the sample. The bulk of these pressure measurements indicated that the reaction front reached the end of the sample opposite the igniter prior to, or coincident with, the arrival of the pressure wave, lending credence to the assumed mechanism of heat transfer by conduction only.

From these comparisons, it is therefore concluded that the two-dimensional model based on the reaction mechanism previously proposed enables predictions of the reaction propagation velocity in heterogeneous lithium-PTFE samples which are in reasonable agreement with experimental results. To argue that the proposed reaction mechanism is, in fact, an accurate representation of the situation under which the chemical reaction actually takes place would be ludicrous. It is, however, observed that acceptably accurate reaction propagation velocities may be predicted from a model based on this mechanism

CHAPTER V

SUMMARY

The overall objective of this study was the investigation of the chemical reaction propagation process occurring in heterogeneous lithium-PTFE reaction samples. This process was examined both analytically and experimentally in order that the reaction propagation velocitymight be predicted and measured.

A reaction mechanism was proposed in which the reaction rate controlling step was assumed to be the thermal decomposition of the PTFE to C_2F_4 gas according to published vacuum pyrolysis rate information. It was postulated that the C_2F_4 produced by the thermal decomposition of the PTFE reacts immediately upon its formation with the lithium to form condensed-phase reaction products. Conduction of heat from the reaction zone through the unreacted lithium and PTFE was assumed to be the sole mode of energy transfer by which these reactants are preheated.

Based on this proposed reaction mechanism, a two-dimensional model was developed. This model, in dimensionless form, was solved numerically to predict the steady dimensionless reaction propagation velocity as a function of the PTFE-lithium mass ratio. Over the range analytically investigated, the predicted value of the steady dimensionless reaction propagation velocity, V_S^*, was observed to decrease with increasing PTFE-lithium mass ratio, M^*, according to the linear relationship:

$$V_S^* = 1.8575 - 1.1536\ M^*$$

The experimental phase of this study involved the use of cylindrical reaction samples through which the reaction front was allowed to propagate axially. The cylindrical PTFE sample was located along the longitudinal centerline of the reaction sample, and was surrounded by the lithium. A test apparatus was developed which allowed the motion of the reaction front to be monitored by means of thermocouples positioned at various axial locations along the lithium-PTFE interface, the reaction having been initiated at one end of the reaction sample by the action of an electric igniter. Reliable reaction propagation data were obtained from test runs in which PTFE samples in the form of solid rod as well as resin were utilized at two different PTFE sample diameters. The propagation of the reaction front was shown to be axisymmetric and crude pressure measurements were made from which it was indicated that the reactants are not preheated by gas-phase convection. The estimated accuracy of the reaction propagation velocity measurements was $\pm$ 15 percent.

From comparison with experimental results, it was demonstrated that the model predicts reaction propagation velocities with acceptable accuracy for the reaction of lithium with PTFE in the form of both solid rod and resin. Better correlation was, however, obtained at the smaller PTFE sample diameter.

The results of this study indicate that several areas are of interest for future investigation. In order to obtain more reliable reaction propagation velocity data with this fuel-oxidizer combination, a more flexible high speed data acquisition system with better time resolution is necessary. Also, an igniter capable of consistently initiating the chemical reaction under all experimental

conditions would be of benefit. The range of PTFE-lithium mass ratios examined with the model should be extended, especially in the direction of lower values of this parameter. The effect on the reaction propagation velocity of the presence of an additional gaseous oxidizer should also be examined. Finally, experimental investigations with other fuels and oxidizers would be of great utility in determining the general validity of the proposed reaction mechanism and the resulting model.

BIBLIOGRAPHY

1. Jones, W. H. (Chairman), JANAF Thermochemical Tables, Dow Chemical Company, Midland, Michigan.

2. Lippmann, D., and Stoltenberg, M. P., "Heat Storage Materials," Lithium Corporation of America, Inc., New York. 1961.

3. "A Compendium of Data on Lithium and Selected Compounds of Lithium," Lithium Corporation of America, Inc., New York, 1959.

4. Tyzak, C., and Longton, P. B., "The Oxidation of Lithium," RDB-C-TN-131, Research and Development Branch, Culcheth Laboratories, Nr. Warrington, Lancs., England, 1955.

5. Longton, P. B., "The Reaction of Lithium with Nitrogen," United Kingdom Atomic Authority, IGR-TN-C-276, Culcheth Laboratories, Nr. Warrington, Lancs., England, 1955.

6. Chandrasekharaiah, M. S., and Margrave, J. L., "The Kinetics of Oxidation and Nitridation of Lithium, Calcium, Strontium, and Barium," J. Electrochem. Soc., 108 (11), 1961, pp. 1008-1012.

7. McFarlane, E. F., and Tompkins, F. C., "Nitridation of Lithium," Trans. Faraday Soc., 58 (5), 1962, pp. 97-1007.

8. Little, T. E., "Reactivity of Nitrogen, Oxygen, and Halogenated Gases with Molten Lithium Metal," The Pennsylvania State University, Ph.D. Thesis, September 1972.

9. Sutton, G. P., Rocket Propulsion Elements, John Wiley and Sons, 1963, pp. 335-357.

10. Summerfield, M., Sutherland, G. S., Webb, M. J., Taback, H. J., and Hall, K. P., "Burning Mechanism of Ammonium Perchlorate Propellants," ARS Progress in Astronautics and Rocketry: Solid Propellant Rocket Research, Summerfield, M., Ed., Academic Press, 1960, pp. 141-182.

11. Fenn, J. B., "A Phalanx Flame Model for the Combustion of Composite Solid Propellants," Combustion and Flame, 12 (3), June 1968, pp. 201-216.

12. Hermance, C. E., "A Model of Composite Propellant Combustion Including Surface Heterogeneity and Heat Generation," AIAA Journal, 4 (9), September 1966, pp. 1629-1637.

13. Culick, F. E. C., and Dehority, G. L., "An Elementary Calculation for the Burning Rate of Composite Solid Propellants," Combustion Science and Technology, 1, 1969, pp. 193-204.

14. Friedman, R., "A Survey of Knowledge about Idealized Fire Spread Over Surfaces," Fire Research Abstracts and Reviews, 10, 1968, pp. 1-8.

15. Magee, R. S., and McAlevy, R. F., "The Mechanism of Flame Spread," J. Fire and Flammability, 2, October 1971, pp. 271-297.

16. Krisnamurthy, L., and Williams, F. A., "Laminar Combustion of Polymethylmethacrylate in O_2/N_2 Mixtures," Fourteenth Symposium (International) on Combustion, The Combustion Institute, Pittsburgh, 1973, pp. 1151-1164.

17. Fernandez-Pello, A., and Williams, F. A., "Laminar Flame Spread Over PMMA Surfaces," Fifteenth Symposium (International) on Combustion, The Combustion Institute, Pittsburgh, 1975, pp. 217-231.

18. Sibulkin, M., and Hansen, A. G., "Flame Spreading Over a Horizontal Fuel Surface," Presented at Eastern Section, The Combustion Institute, 1974 Fall Meeting, Silver Spring, Maryland.

19. Frey, A. E., and T'ien, J. S., "Near Limit Flame Spread Over Cellulosic Materials," Presented at Eastern Section, The Combustion Institute, 1974 Fall Meeting, Silver Spring, Maryland.

20. Markstein, G. H., and de Ris, J., "Flame Spread Along Fuel Edges," Presented at Eastern Section, The Combustion Institute, 1974 Fall Meeting, Silver Spring, Maryland.

21. McAlevy, R. F., and Magee, R. S., "The Mechanism of Flame Spreading Over the Surface of Igniting Condensed-Phase Materials," Twelfth Symposium (International) on Combustion, The Combustion Institute, Pittsburgh, 1969, pp. 215-226.

22. Lastrina, F. A., Magee, R. S., and McAlevy, R. F., "Flame Spread Over Fuel Beds: Solid-Phase Energy Considerations," Thirteenth Symposium (International) on Combustion, The Combustion Institute, Pittsburgh, 1971, pp. 935-946.

23. de Ris, J. N., "Spread of a Laminar Diffusion Flame," Twelfth Symposium (International) on Combustion, The Combustion Institute, Pittsburgh, 1969, pp. 241-249.

24. Tarifa, C. S., Notario, P. P. D., and Terralbo, A. M , "On the Process of Flame Spreading Over the Surface of Plastic Fuels in an Oxidizing Atmosphere," Twelfth Symposoum (International) on Combustion, The Combustion Institute, Pittsburgh, 1969, pp 229-240.

25. Feng, C. C., and Sirignano, W. A., "Further Calculations Based Upon a Theory of Flame Spread Across Solid Fuels," Presented at Eastern Section, The Combustion Institute, 1974 Fall Meeting, Silver Spring, Maryland.

26. Akita, K., "Some Problems of Flame Spread Along a Liquid Surface," Fourteenth Symposium (International) on Combustion, The Combustion Institute, Pittsburgh, 1973, pp. 1075-1082.

27. Helmstetter, A., Dryer, F. L., and Glassman, I., "An Experimental Study of Flame Spreading Over Liquid Fuels," Presented at Eastern Section, The Combustion Institute, 1974 Fall Meeting, Silver Spring, Maryland.

28. Leber, S., and Hehemann, R. F., "Homogenization Kinetics of a Sintered Columbium Alloy," Transactions of the Metallurgical Society of AIME, 230, 1964, pp. 100-106.

29. Smith, D. W., and Hehemann, R. F., "Kinetics of Alloy Formation in Sintered Tungsten-Rhenium Powder Compacts," Transactions of the Metallurgical Society of AIME, 236, 1966, pp. 506-512.

30. Fisher, B., and Rudman, P. S., "X-Ray Diffraction Study of Interdiffusion in Cu-Ni Powder Compacts," Journal of Applied Physics, 32 (8) 1961, pp. 1604-1611.

31. Hardt, A. P., and Phung, P. V., "Propagation of Gasless Reactions in Solids-I. Analytical Study of Exothermic Intermetallic Reaction Rates," Combustion and Flame, 21, 1973, pp. 77-89.

32. Hardt, A. P., and Holsinger, R. W., "Propagation of Gasless Reactions in Solids-II. Experimental Study of Exothermic Intermetallic Reaction Rates," Combustion and Flame, 21, 1973, pp. 91-97.

33. Product Bulletin, "F-ND Magnesium/TFE Ignition Materials," Atlantic Research Corporation, Ordnance Division, Alexandria, Virginia.

34. Griffiths, V. S., O'Sullivan, E. F., and Thackeray, D. P. C., "Observations on the Combustion of Magnesium-Polytetrafluoroethane Pyrotechnic Pellets," University of Surrey, Guildford, England, 1974, unpublished paper

35. Madorsky, S. L., Hart, V. E., Straus, S., and Sedlak, V. A., "Thermal Degradation of Tetrafluoroethylene and Hydrofluoroethylene Polymers in a Vacuum," Journal of Research of the National Bureau of Standards, 51 (6), 1953, pp. 327-333.

36. Wall, L. A., and Michaelsen, J. D., "Thermal Decomposition of Polytetrafluoroethylene in Various Gaseous Atmospheres," Journal of Research of the National Bureau of Standards, 56 (1), 1956, pp. 27-34.

37. Siegle, J. C., Muus, L. T., Lin, T. P., and Larsen, H. A., The Molecular Structure of Perfluorocarbon Polymers, II. Pyrolysis of Polytetrafluoroethylene," Journal of Polymer Science, Part A, 2, 1964, pp. 391-404.

38. Siegle, J. C., and Muus, L. T., "Pyrolysis of Polytetrafluoroethylene," Presented at the September 17, 1956 Meeting of the American Chemical Society.

39. Holman, J. P., Heat Transfer, McGraw-Hill, 1963.

40. Smith, G. D., Numerical Solution of Partial Differential Equations, Oxford University Press, 1965.

41. Kunz, K. S., Numerical Analysis, McGraw-Hill, 1957.

42. Davison, H. W., "Compilation of Thermophysical Properties of Liquid Lithium," NASA TN D-4650, 1968.

43. "The Journal of Teflon, Reprint No. 41," E. I. duPont de Nemours and Company (Incorporated), Plastics Department, Fluorocarbons Division, Wilmington, Delaware.

44. Streenivasan, K., and Altman, M., "The Determination of Thermal Diffusivities of Thermal Energy Storage Materials. Part II - Molten Salts Beyond the Melting Point," Transactions of the ASME, Journal of Engineering for Power, July 1969, pp. 189-197.

APPENDIX A

DERIVATION OF THE FINITE DIFFERENCE EXPRESSIONS

During the transformation of the dimensionless heat conduction equations, Equations (2.16) and (2.18), into finite difference form for numerical solution, three different types of grid patterns were encountered. These three patterns are shown in Figure 15, and consist of regular grid patterns at interior grid points, Figure 15(a), grid patterns at spatial boundaries, Figure 15(b), and grid patterns with unequal grid spacing such as present at the lithium-PTFE interface, Figure 15(c). The derivations of the finite difference expressions approximating the partial differential equations for each of these cases are illustrated in the following examples. For ease of notation, the * superscripts present in the original equations are omitted; superscripts in the following expressions refer to dimensionless time level and subscripts to spatial location.

For regular grid patterns at interior grid points in the stoichiometric lithium, as shown in Figure 15(a), finite difference expressions approximating the solution of Equation (2.18),

$$\frac{\partial T}{\partial \tau} = \Lambda \left(\frac{\partial^2 T}{\partial X^2} + \frac{\partial^2 T}{\partial Y^2} \right) , \tag{2.18}$$

may be arrived at by first writing a Taylor's Series expansion about the grid point, i, j, as follows, all derivatives being evaluated at grid point i, j:

$$T^N_{i+1,j} = T^N_{i,j} + \Delta X \frac{\partial T}{\partial X} + \frac{\Delta X^2}{2!} \frac{\partial^2 T}{\partial X^2} + \frac{\Delta X^3}{3!} \frac{\partial^3 T}{\partial X^3} + \ldots , \tag{A.1}$$

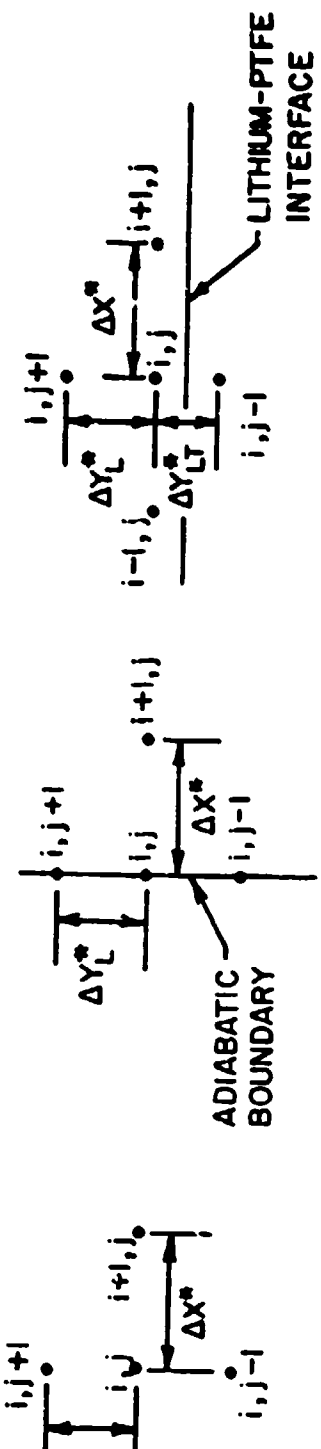

Figure 15 Sketch of Finite Difference Grid Patterns

$$T^N_{i-1,j} = T^N_{i,j} - \Delta X \frac{\partial T}{X} + \frac{\Delta X^2}{2!} \frac{\partial^2 T}{\partial X^2} - \frac{\Delta X^3}{3!} \frac{\partial^3 T}{\partial X^3} + \ldots, \qquad (A.2)$$

$$T^N_{i,j+1} = T^N_{i,j} + \Delta Y_L \frac{\partial T}{\partial Y} + \frac{\Delta Y_L^2}{2!} \frac{\partial^2 T}{\partial Y^2} + \frac{\Delta Y_L^3}{3!} \frac{\partial^3 T}{\partial Y^3} + \ldots, \qquad (A.3)$$

$$T^N_{i,j-1} = T^N_{i,j} - \Delta Y_L \frac{\partial T}{\partial Y} + \frac{\Delta Y_L^2}{2!} \frac{\partial^2 T}{\partial Y^2} - \frac{\Delta Y_L^3}{3!} \frac{\partial^3 T}{\partial Y^3} + \ldots . \qquad (A.4)$$

It is desired to add the above four equations in such a manner as to arrive at a finite difference expression approximating the spatial derivatives on the right-hand side of Equation (2.18). Accordingly, Equations (A.1) through (A.4) are multiplied by the constants C_1, C_2, C_3 and C_4, respectively. The following constraints are then necessary in order for the addition to yield the desired results:

$$\sum \text{coefficients of } \frac{\partial^2 T}{\partial X^2} = 1 \quad ,$$

$$\sum \text{coefficients of } \frac{\partial T}{\partial X} = 0 \quad ,$$

$$\sum \text{coefficients of } \frac{\partial^2 T}{\partial Y^2} = 1 \quad ,$$

$$\sum \text{coefficients of } \frac{\partial T}{\partial Y} = 0 \quad . \qquad (A.5)$$

These constraints applied to the addition of Equations (A.1) through (A.4) then yield:

$$\frac{\Delta X^2}{2!} (C_1 + C_2) = 1 \quad ,$$

$$\Delta X (C_1 - C_2) = 0 \quad ,$$

$$\frac{\Delta Y_L^2}{2!} (C_3 + C_4) = 1 \quad ,$$

$$\Delta Y_L (C_3 - C_4) = 0 \qquad (A.6)$$

Solution of Equation (A.6) yields:

$$C_1 = C_2 = \frac{1}{\Delta X^2}$$

and

$$C_3 = C_3 = \frac{1}{\Delta Y_1^2} \quad . \tag{A.7}$$

Multiplying Equations (A.1) through (A.4) by the constants C_1 through C_4 as given by Equations (A.7), respectively, adding the resulting expressions, and neglecting terms involving the fourth-and-higher order derivatives gives:

$$\frac{\partial^2 T}{\partial X^2} + \frac{\partial^2 T}{\partial Y^2} = \frac{1}{\Delta X^2}\left(T^N_{i+1,j} + T_{i-1,j} - 2T^N_{i,j}\right) + \frac{1}{\Delta Y_1^2}\left(T^N_{i,j+1} + T^N_{i,j-1} - 2T^N_{i,j}\right). \tag{A.8}$$

The dimensionless time derivative on the left-hand side of Equation (2.18) is then approximated by the forward difference expression [40]:

$$\frac{\partial T}{\partial \tau} = \frac{T^{N+1}_{i,j} - T^N_{i,j}}{\Delta \tau} \quad . \tag{A.9}$$

Multiplying Equation (A.8) by the dimensionless coefficient A*, and equating the resulting expression with Equation (A.9) yields the following finite difference approximation for Equation (2.18):

$$\frac{T^{N+1}_{i,j} - T^N_{i,j}}{\Delta \tau} = \frac{A_{i,j}}{\Delta X^2}\left(T^N_{i+1,j} + T^N_{i-1,j} - 2T^N_{i,j}\right) + \frac{A_{i,j}}{\Delta Y_L^2}\left(T^N_{i,j+1} + T^N_{i,j-1} - 2T^N_{i,j}\right). \tag{A.10}$$

This equation may then be rearranged to give an explicit expression for the dimensionless temperature at grid point i,j at dimensionless

time level N+1, in terms of the dimensionless temperatures at grid point i,j and the four adjacent grid points at dimensionless time level N as follows:

$$T_{i,j}^{N+1} = \frac{A_{i,j}\Delta\tau}{\Delta X^2}\left(T_{i+1,j}^{N} + T_{i-1,j}^{N} - 2T_{i,j}^{N}\right) + \frac{A_{i,j}\Delta\tau}{\Delta Y_L^{\,2}}\left(T_{i,j+1}^{N} + T_{i,j-1}^{N} - 2T_{i,j}^{N}\right) + T_{i,j}^{N} \quad . \qquad (A.11)$$

The finite difference approximation for Equation (2.16), which includes a heat generation term, at interior grid point i,j in the PTFE is derived in a like manner to give:

$$T_{i,j}^{N+1} = \frac{A_{i,j}\Delta\tau}{\Delta X^2}\left(T_{i+1,j}^{N} + T_{i-1,j}^{N} - 2T_{i,j}^{N}\right) + \frac{A_{i,j}\Delta\tau}{\Delta Y_T^{\,2}}\left(T_{i,j+1}^{N} + T_{i,j-1}^{N} - 2T_{i,j}^{N}\right) + T_{i,j}^{N} - R\Delta\tau\,\frac{dZ_{Ti,j}^{N}}{d\tau} \quad , \qquad (A.12)$$

where:

$$\frac{dZ_{Ti,j}^{N}}{d\tau} = -\,FZ_{Ti,j}^{N}\, e^{-E/T_{i,j}^{N}} \quad . \qquad (A.13)$$

For grid points on spatial boundaries as shown in Figure 15(b) which are assumed to be adiabatic, finite difference expressions approximating the solution of Equation (2.18) are derived by again writing a Taylor's Series expansion around grid point i,j in the stoichiometric lithium as follows, all derivatives being evaluated at grid point i,j:

$$T_{i+1,j}^{N} = T_{i,j}^{N} + \Delta X\,\frac{\partial T}{\partial X} + \frac{\Delta X^2}{2!}\,\frac{\partial^2 T}{\partial X^2} + \frac{\Delta X^3}{3!}\,\frac{\partial^3 T}{\partial X^3} + \ldots , \qquad (A.14)$$

$$T^N_{i,j+1} = T^N_{i,j} + \Delta Y_L \frac{\partial T}{\partial Y} + \frac{\Delta Y_L^2}{2!} \frac{\partial^2 T}{\partial Y^2} + \frac{\Delta Y_L^3}{3!} \frac{\partial^3 T}{\partial Y^3} + \ldots, \quad (A.15)$$

$$T^N_{i,j-1} = T^N_{i,j} - \Delta Y_L \frac{\partial T}{\partial Y} + \frac{\Delta Y_L^2}{2!} \frac{\partial^2 T}{\partial Y^2} - \frac{\Delta Y_L^3}{3!} \frac{\partial^3 T}{\partial Y^3} + \ldots . \quad (A.16)$$

Noting that at an adiabatic boundary as shown in Figure 15(b), $\frac{\partial T}{\partial X} = 0$, and neglecting terms involving third-and-higher order derivatives allows Equation (A.14) to be rearranged to yield an expression for $\frac{\partial^2 T}{\partial X^2}$. It being desired to add Equations (A.15) and (A.16) to give an expression for $\frac{\partial^2 T}{\partial Y^2}$, these equations are first multiplied by constants C_5 and C_6, respectively. The values of these constants are determined, through constraints on the sums of the coefficients of $\frac{\partial^2 T}{\partial Y^2}$ and $\frac{\partial T}{\partial Y}$, to be:

$$C_5 = C_6 = \frac{1}{\Delta Y_L^2} \quad . \quad (A.17)$$

Multiplying Equations (A.15) and (A.16) by C_5 and C_6 as given above, adding the resulting expressions while neglecting fourth-and-higher order derivatives, and introducing the expression for $\frac{\partial^2 T}{\partial X^2}$ yields:

$$\frac{\partial^2 T}{\partial X^2} + \frac{\partial^2 T}{\partial Y^2} = \frac{2}{\Delta X^2} \left(T^N_{i+1,j} - T^N_{i,j} \right) + \frac{1}{\Delta Y_L^2} \left(T^N_{i,j+1} + T^N_{i,j-1} - 2T^N_{i,j} \right) , \quad (A.18)$$

for a grid point i,j on a spatial boundary as shown in Figure 15(b). Expressing the dimensionless time derivative as given in Equation (A.9), multiplying Equation (A.18) by the dimensionless parameter A*, equating these two expressions and rearranging gives the following equation for the dimensionless temperature of boundary grid point i,j in the stoichiometric lithium at the N+1 time level:

$$T^{N+1}_{i,j} = \frac{2A_{i,j}\Delta\tau}{\Delta X^2}\left(T^N_{i+1,j} - T^N_{i,j}\right) + \frac{A_{i,j}\Delta\tau}{\Delta Y_L^2}\left(T^N_{i,j+1} + T^N_{i,j-1} - 2T^N_{i,j}\right) + T^N_{i,j} \quad . \qquad (A.19)$$

In a similar manner, a finite difference approximation for Equation (2.16) at a spatial boundary grid point i,j in the PTFE layer may be derived to give:

$$T^{N+1}_{i,j} = \frac{2A_{i,j}\Delta\tau}{\Delta X^2}\left(T^N_{i+1,j} - T^N_{i,j}\right) + \frac{A_{i,j}\Delta\tau}{\Delta Y_L^2}\left(T^N_{i,j+1} + T^N_{i,j-1} - 2T^N_{i,j}\right) + T^N_{i,j} - R\Delta\tau\,\frac{dZ^N_{Ti,j}}{d\tau} \quad , \qquad (A.20)$$

where

$$\frac{dZ^N_{Ti,j}}{d\tau} = -FZ^N_{Ti,j}\, e^{-E/T^N_{i,j}} \quad . \qquad (A.13)$$

For grid points in the stoichiometric lithium which are adjacent to the lithium-PTFE interface, as shown in Figure 15(c), finite difference expressions approximating the solution of Equation (2.18) may also be arrived at by writing a Taylor's Series expansion about grid point i,j as follows, all derivatives being evaluated at grid point i,j:

$$T^N_{i+1,j} = T^N_{i,j} + \Delta X\,\frac{\partial T}{\partial X} + \frac{\Delta X^2}{2!}\,\frac{\partial^2 T}{\partial X^2} + \frac{\Delta X^3}{3!}\,\frac{\partial^3 T}{\partial X^3} + \ldots, \qquad (A.21)$$

$$T^N_{i-1,j} = T^N_{i,j} - \Delta X\,\frac{\partial T}{\partial X} + \frac{\Delta X^2}{2!}\,\frac{\partial^2 T}{\partial X^2} - \frac{\Delta X^3}{3!}\,\frac{\partial^3 T}{\partial X^3} + \ldots, \qquad (A.22)$$

$$T^N_{i,j+1} = T^N_{i,j} + \Delta Y_L\,\frac{\partial T}{\partial Y} + \frac{\Delta Y_L^2}{2!}\,\frac{\partial^2 T}{\partial Y^2} + \frac{\Delta Y_L^3}{3!}\,\frac{\partial^3 T}{\partial Y^3} + \ldots, \qquad (A.23)$$

$$T^N_{i,j-1} = T^N_{i,j} - \Delta Y_{LT}\frac{\partial T}{\partial Y} + \frac{\Delta Y_{LT}^2}{2!}\frac{\partial^2 T}{\partial Y^2} - \frac{\Delta Y_{LT}^3}{3!}\frac{\partial^3 T}{\partial Y^3} + \ldots . \tag{A.24}$$

It being again desired to add the above four equations to arrive at a finite difference approximation for the spatial derivatives on the right-hand side of Equation (2.18), Equations (A.21) through (A.24) are multiplied by constants C_7 through C_{10}, respectively. The values of these constants are then determined by the constraints given by Equations (A.5) to be:

$$C_7 = C_8 = -\frac{1}{\Delta X^2} ,$$

$$C_9 = \frac{2}{\Delta Y_{LT}\Delta Y_L\left(1 + \frac{\Delta Y_L}{\Delta Y_{LT}}\right)} ,$$

$$C_{10} = \frac{2}{\Delta Y_{LT}^2\left(1 + \frac{\Delta Y_L}{\Delta Y_{LT}}\right)} . \tag{A.25}$$

Multiplying Equations (A.21) through (A.24) by constants C_7 through C_{10}, respectively, adding the resulting expressions, and neglecting terms involving third-and-higher order derivatives yields:

$$\frac{\partial^2 T}{\partial X^2} + \frac{\partial^2 T}{\partial Y^2} = \frac{1}{\Delta X^2}\left(T^N_{i+1,j} + T^N_{i-1,j} - 2T^N_{i,j}\right) + C_9\left(T^N_{i,j+1} - T^N_{i,j}\right) + C_{10}\left(T^N_{i,j-1} - T^N_{i,j}\right) , \tag{A.26}$$

where the values of C_9 and C_{10} are given by Equations (A.25). Multiplying Equation (A.26) by the dimensionless parameter A*,

representing the dimensionless time derivative in Equation (2.18) as shown in Equation (A.9), equating and rearranging gives the following expression for the dimensionless temperature at grid point i,j in the stoichiometric lithium adjacent to the lithium-PTFE interface at dimensionless time level N+1:

$$T_{i,j}^{N+1} = \frac{A_{i,j}\Delta\tau}{\Delta X^2}\left(T_{i+1,j}^{N} + T_{i-1,j}^{N} - 2T_{i,j}^{N}\right) + C_9\, A_{i,j}\Delta\tau\left(T_{i,j+1}^{N} - T_{i,j}^{N}\right) + C_{10}\, A_{i,j}\Delta\tau\left(T_{i,j-1}^{N} - T_{i,j}^{N}\right) + T_{i,j}^{N} \quad , \tag{A.27}$$

where C_9 and C_{10} are given by Equations (A.25). Similarly, a finite difference approximation for Equation (2.16) at grid point i,j in the PTFE adjacent to the lithium-PTFE interface may be derived to yield:

$$T_{i,j}^{N+1} = \frac{A_{i,j}\Delta\tau}{\Delta X^2}\left(T_{i+1,j}^{N} + T_{i-1,j}^{N} - 2T_{i,j}^{N}\right) + C_{11}\, A_{i,j}\Delta\tau\left(T_{i,j+1}^{N} - T_{i,j}^{N}\right) + C_{12}\, A_{i,j}\Delta\tau\left(T_{i,j-1}^{N} - T_{i,j}^{N}\right) + T_{i,j}^{N} - R\Delta\tau\,\frac{dZ_{Ti,j}^{N}}{d\tau} \quad , \tag{A.28}$$

where

$$C_{11} = \frac{2}{\Delta Y_{LT}\Delta Y_T\left(1 + \frac{\Delta Y_{LT}}{\Delta Y_T}\right)} \quad ,$$

$$C_{12} = \frac{2}{\Delta Y_T^{\,2}\left(1 + \frac{\Delta Y_{LT}}{\Delta Y_T}\right)}$$

and

$$\frac{dZ_{Ti,j}^{N}}{d\tau} = -FZ_{Ti,j}^{N}\, e^{-E/T_{i,j}^{N}} \quad . \tag{A.13}$$

The equations used in the numerical solution of the dimensionless form of the two-dimensional model, Equations (2.16) through (2.20) were either identical to those presented in this appendix, or combinations of two of the examples illustrated.

APPENDIX B

COMPUTER PROGRAM FLOW DIAGRAM

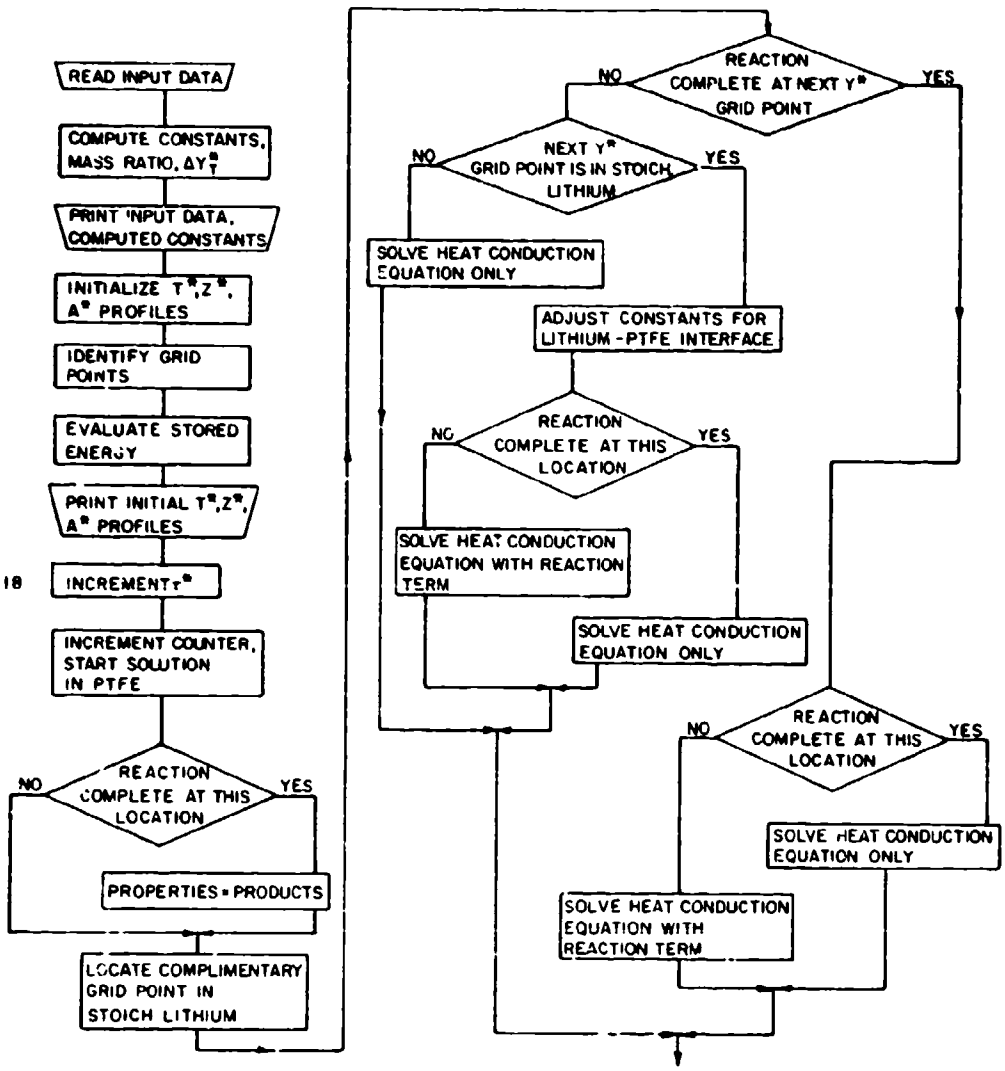

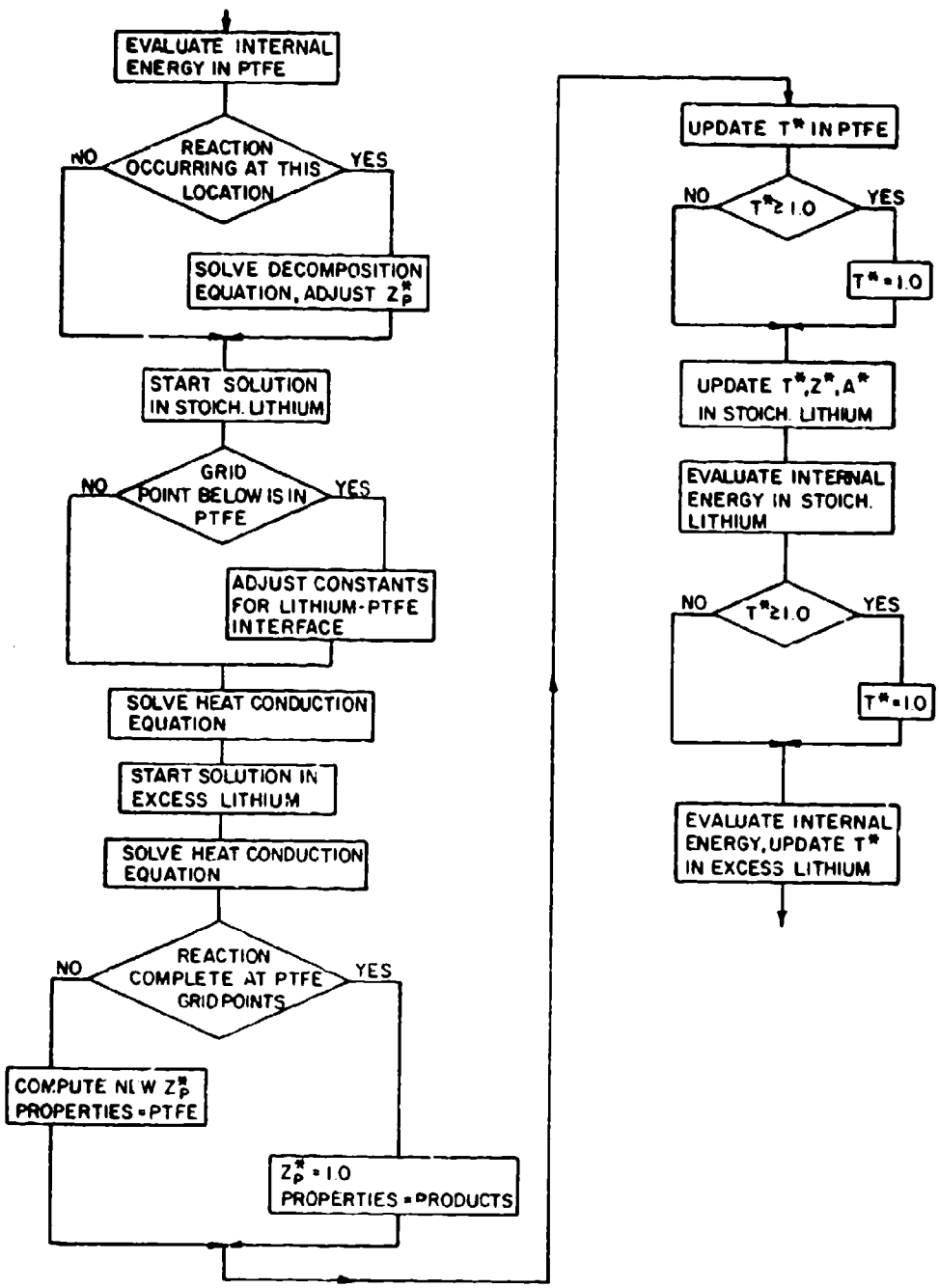
EVALUATE INTERNAL ENERGY IN PTFE
REACTION OCCURRING AT THIS LOCATION
NO
YES
SOLVE DECOMPOSITION EQUATION, ADJUST Z_p^*
START SOLUTION IN STOICH. LITHIUM
GRID POINT BELOW IS IN PTFE
NO
YES
ADJUST CONSTANTS FOR LITHIUM-PTFE INTERFACE
SOLVE HEAT CONDUCTION EQUATION
START SOLUTION IN EXCESS LITHIUM
SOLVE HEAT CONDUCTION EQUATION
REACTION COMPLETE AT PTFE GRID POINTS
NO
YES
COMPUTE NEW Z_p^* PROPERTIES = PTFE
$Z_p^* = 1.0$ PROPERTIES = PRODUCTS
UPDATE T^* IN PTFE
$T^* \geq 1.0$
NO
YES
$T^* = 1.0$
UPDATE T^*, Z^*, A^* IN STOICH. LITHIUM
EVALUATE INTERNAL ENERGY IN STOICH. LITHIUM
$T^* \geq 1.0$
NO
YES
$T^* = 1.0$
EVALUATE INTERNAL ENERGY, UPDATE T^* IN EXCESS LITHIUM

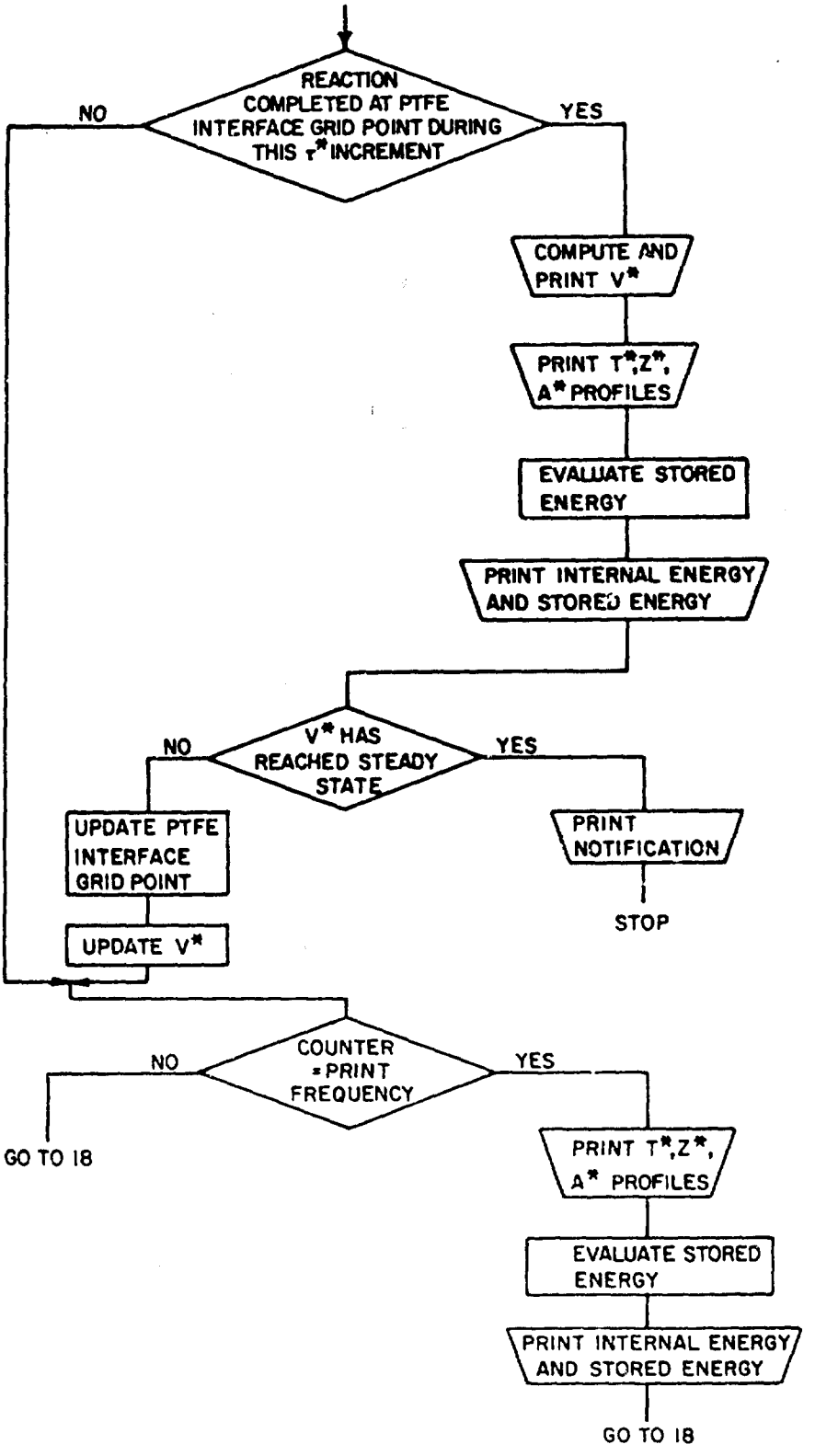

APPENDIX C

PHYSICAL AND CHEMICAL PROPERTIES

The values of the physical and chemical properties used in the numerical solution of the model are summarized in Table 6.

Table 6

Values of Physical and Chemical Properties Used in the Model

Property	Value	Source
A_o	3.0×10^{19} s^{-1}	Reference [37]
C_{P_L}	4.187×10^3 J/kg-K	Reference [42]
C_{P_P}	2.470×10^3 J/kg-K	Reference [1]
C_{P_T}	1.047×10^3 J/kg-K	Reference [43]
E_a	3.475×10^5 J/mol	Reference [37]
ΔH_R	1.237×10^7 J/kg reactants	Computed using References [1] and [37]
k_L	55.45 W/m-K	Reference [42]
k_P	1.731 W/m-K	Reference [44]
k_T	0.2527 W/m-K	Reference [43]
T_{af}	1966 K	Computed using References [1], [2] and [37]
W	1.416	Computed using Reference [1]
ρ_L	481 kg/m^3	Reference [42]
ρ_P	1110 kg/m^3	Computed using References [1], [42] and [43]
ρ_T	2160 kg/m^3	Reference [43]

VITA

Richard Bryant Smith was born on January 31, 1945, in Scranton, Pennsylvania. In May, 1963, he was graduated from Elk Lake Joint High School in Dimock, Pennsylvania. He received the degree of Bachelor of Science in Mechanical Engineering in June, 1967, from The University of Maryland, and the degree of Master of Science in Mechanical Engineering from The Pennsylvania State University in December, 1969.

From October, 1968, to the present, Mr. Smith has been employed as a Research Assistant at the Applied Research Laboratory of The Pennsylvania State University. He is a member of Tau Beta Pi, Pi Tau Sigma, and Sigma Xi.